

Review

# Recent Advances in Design Strategies and Imaging Applications of Fluorescent Probes for ATP

Qing-Song Gu<sup>1</sup>, Ting Li<sup>1</sup>, Ting Liu<sup>1</sup>, Guo Yu<sup>1</sup>, Guo-Jiang Mao<sup>2</sup>, Fen Xu<sup>1</sup> and Chun-Yan Li<sup>1,\*</sup>

<sup>1</sup> Key Laboratory for Green Organic Synthesis and Application of Hunan Province, Key Laboratory of Environmentally Friendly Chemistry and Applications of Ministry of Education, College of Chemistry, Xiangtan University, Xiangtan 411105, China; guqingsong365@outlook.com (Q.-S.G.); liting170928@outlook.com (T.L.); 202005601128@smail.xtu.edu.cn (T.L.); 202005601116@smail.xtu.edu.cn (G.Y.); xufen@xtu.edu.cn (F.X.)

<sup>2</sup> Henan Key Laboratory of Organic Functional Molecule and Drug Innovation, Collaborative Innovation Center of Henan Province for Green Manufacturing of Fine Chemicals, Key Laboratory of Green Chemical Media and Reactions, Ministry of Education, School of Chemistry and Chemical Engineering, Henan Normal University, Xinxiang 453007, China; maoguojiang@htu.edu.cn

\* Correspondence: lichunyan79@sina.com

**Abstract:** Adenosine 5'-triphosphate (ATP) is the energy currency in cells. It is involved in numerous cellular life activities and exhibits a close association with the development of certain diseases. Thus, the precise detection of ATP within cells holds immense significance in understanding cell biological events and related disease development. Fluorescent probes have obvious advantages in imaging ATP in cells and in vivo due to their high sensitivity, good selectivity, real-time imaging, and good biocompatibility. Thus far, an extensive array of fluorescent probes targeting ATP has been formulated to enable the visualization of ATP within cells and in vivo. This review summarizes the recent advances in ATP fluorescent probes according to different design strategies, mainly including those based on organic small molecules, metal complexes, and water-soluble conjugated polymers. In addition, the practical applications of ATP fluorescent probes in the imaging of target organelles, cell biological events, and disease markers are highlighted. Finally, the challenges and future trends of ATP detection based on fluorescent probes are discussed.

**Keywords:** fluorescent probes; adenosine 5'-triphosphate (ATP); design strategy; imaging application



**Citation:** Gu, Q.-S.; Li, T.; Liu, T.; Yu, G.; Mao, G.-J.; Xu, F.; Li, C.-Y. Recent Advances in Design Strategies and Imaging Applications of Fluorescent Probes for ATP. *Chemosensors* **2023**, *11*, 417. <https://doi.org/10.3390/chemosensors11070417>

Academic Editor: Guo-Hui Pan

Received: 6 June 2023

Revised: 19 July 2023

Accepted: 21 July 2023

Published: 24 July 2023



**Copyright:** © 2023 by the authors. Licensee MDPI, Basel, Switzerland. This article is an open access article distributed under the terms and conditions of the Creative Commons Attribution (CC BY) license (<https://creativecommons.org/licenses/by/4.0/>).

## 1. Introduction

Adenosine 5'-triphosphate (ATP) is an important biological molecule, which is the main source of energy for cells. It participates in a variety of life processes, including protein synthesis, ion transport in cells, neurotransmission, cell division, and glycolysis [1–7]. An abnormal level of ATP metabolism is related to many diseases, such as ischemia, Parkinson's disease, cardiovascular disease, malignant tumors, and so on [8–13]. In order to study the cellular life process and explore ATP-related diseases, it is of great significance to detect the content and dynamic changes in ATP in biological samples.

Currently, ATP can be detected using various methods, including high-performance liquid chromatography (HPLC), ion chromatography, mass spectrometry, electrochemistry, and bioluminescence analysis [14–17]. However, these analytical methods have the disadvantage of low sensitivity. Fluorescence probes, with many advantages such as high sensitivity, excellent spatial and temporal resolution, and real-time in situ imaging, have emerged as crucial tools for the detection and imaging of bio-active substances during medical diagnosis [18–31]. Moreover, near-infrared (NIR) fluorescent probes have long excitation/emission wavelengths that allow deeper tissue penetration while reducing the background fluorescence of proteins and photodamage to biological samples [32–44].

The fluorescent probes for ATP are mainly composed of organic fluorophores and ATP recognition sites. Among them, the interaction between ATP and the recognition

site causes a structural change or energy transfer of the organic fluorophore, which leads to the generation or quenching of fluorescence. The design of ATP fluorescent probes necessitates the careful consideration of several factors. The first is the excitation/emission wavelength of the probe, and longer excitation and emission wavelengths are beneficial for ATP detection in deep biological samples. The second is the selectivity of the probe, and the detection process should only respond to ATP. The third is the appropriate detection range; ATP concentration in cells is usually 1–10 mM and too low or too high a detection range will fail to dynamically image fluctuations in intracellular ATP levels. Fourth, if they are used for the detection of ATP in cells, the probes need to have good biocompatibility. Last but not least, by introducing targeting groups into the probe, it is possible for the probe to have organelle or specific cell-targeting capabilities, which allows the targeted detection of cell biological events and insight into the complex functions of ATP. So far, there has been significant progress in the design and application of ATP fluorescent probes, and many ATP fluorescent probes have been reported [45–48].

In this review, we aim to summarize recent advances in the detection of ATP with fluorescent probes. The ATP fluorescent probes in this paper are categorized into three groups based on different design strategies: organic small molecules, metal complexes, and water-soluble conjugated polymers (Figure 1). This review also highlights the application of ATP fluorescence probes in targeting organelles, imaging cell biological events, and detecting disease markers. Finally, the current challenges in ATP detection and the prospects for the development of ATP fluorescent probes are discussed.

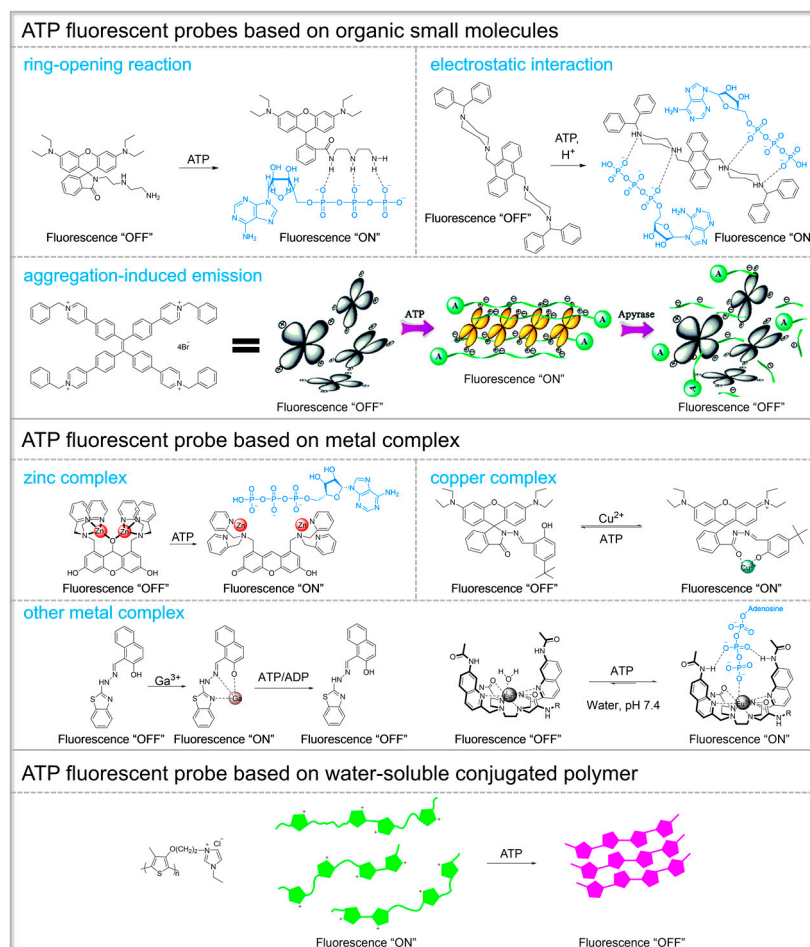


**Figure 1.** The design strategy of fluorescent probes for ATP.

## 2. The Design Strategy of Fluorescent Probes for ATP

### 2.1. ATP Fluorescent Probes Based on Organic Small Molecules

Fluorescent probes for ATP based on organic small molecules have been of great interest because of their good selectivity, high sensitivity, and ease of crossing the cell membrane into cells. Many organic small-molecule fluorescent probes for ATP recognition have been developed and reported. These probes have three main mechanisms, including ring-opening reaction, electrostatic interaction, and aggregation-induced luminescence (AIE).

#### 2.1.1. ATP Fluorescent Probe Based on the Ring-Opening Reaction

Rhodamine dyes are widely utilized as fluorescent probes due to their advantageous properties, such as a high molar extinction coefficient, long emission wavelength, excellent fluorescence quantum yield, and exceptional photostability [49,50]. Rhodamine derivatives with a spirolactam ring structure exhibit non-fluorescent characteristics. When they are exposed to ATP, the spirolactam ring undergoes opening, resulting in a significant enhancement in fluorescence intensity. In recent years, the development of ATP fluorescent probes based on the rhodamine ring-opening reaction has received great attention.

In 2013, a rhodamine spirolactam derivative (probe 1, Figure 2) was developed as a colorimetric and fluorescent chemosensor for ATP [51], and the sensing process is ATP-induced spirolactam ring opening of rhodamine derivatives. Probe 1 itself has no fluorescence emission since rhodamine is in the form of a spirolactam ring in this probe. Upon the introduction of ATP, hydrogen bonds are formed between the diethylenetriamine moiety of probe 1 and the polyphosphates within ATP. Consequently, the configuration of the rhodamine molecule undergoes a transformation from a spirolactam ring to an open-ring amide structure. Thus, the fluorescence signal is activated. Probe 1 has a highly sensitive “turn-on” fluorescence response to ATP. Most importantly, probe 1 successfully overcomes the challenge of significant interference caused by other nucleoside polyphosphates (NPPs) like ADP and AMP. Moreover, this probe can be effectively employed for the fluorescence-based detection of protein kinase activity.

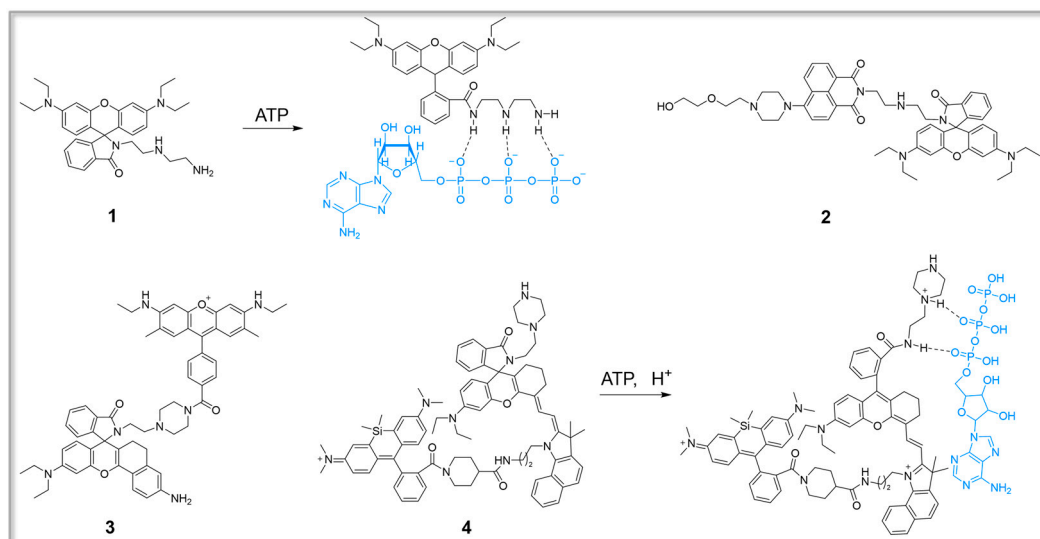


**Figure 2.** Structures and response mechanisms of fluorescent probes 1–4.

In 2014, a ratiometric fluorescent probe (probe 2, Figure 2) for ATP detection was developed based on the Förster resonance energy transfer (FRET) mechanism [52]. In probe 2, the naphthalimide fluorophore is incorporated as the energy donor, while rhodamine serves as the energy acceptor. Due to the spirolactam ring form of the rhodamine moiety in probe 2, only the naphthalimide moiety exhibits the emission. However, upon the addition of ATP, the formation of the probe 2–ATP complex induces a conformational

change in the rhodamine moiety, transitioning it from a spirolactam ring to an open-ring amide structure. This conformational change enables a viable FRET process, facilitating energy transfer from the naphthalimide moiety (energy donor) to the rhodamine moiety (energy acceptor). Consequently, the emission from the naphthalimide decreases, while the emission from the rhodamine becomes apparent, resulting in a noticeable shift from green emission to red emission. By simultaneously interacting with the polyphosphate chain and the nucleic base group, its selectivity for ATP is unexpectedly higher than for other organophosphate anions.

In 2020, a ratiometric fluorescent probe **3** (Figure 2) was designed and synthesized for quantitatively detecting the fluctuation of mitochondrial ATP [53]. Probe **3** was designed based on the FRET mechanism. Rh6G was chosen as the donor fluorophore because of its specific localization to mitochondria and spectral overlap with the dye ACF. In addition, a multisite binding strategy was used to improve selectivity. The incorporation of either two saturated carbon linkers or a rigid piperazine ring facilitates the formation of hydrogen bonds with the phosphate group of ATP. Additionally, it promotes the  $\pi$ - $\pi$  interaction between the nitrogenous bases and the ACF dye. This establishes the conditions for the rapid response of probe **3** to ATP. In addition, probe **3** can discriminate between normal and cancer cell lines by ATP detection.

In 2021, a near-infrared (NIR) reversible probe **4** (Figure 2) was developed for the ratiometric imaging of tumors [54]. In FRET-based probe **4**, the energy donor is silicon rhodamine, while the energy acceptor is CS dye. The probe is designed with an ATP/H<sup>+</sup> recognition unit that remains inactive until both H<sup>+</sup> and ATP molecules are bound to the acceptor. The spirolactam of probe **4** opens after the reaction, activating both ratiometric fluorescence and photoacoustic signals. The probe demonstrates reversible activation upon the binding of both H<sup>+</sup> and ATP molecules. In addition, probe **4** has been successfully employed in tumor photoacoustic and ratiometric fluorescence imaging, as well as fluorescence-imaging-guided tumor resection.

#### 2.1.2. ATP Fluorescent Probe Based on Electrostatic Interaction

Electrostatic interactions involve the formation of hydrogen bonds between the oxygen atoms of the ATP phosphate group and the active hydrogen of the probe. These interactions induce structural changes in the probe, consequently impacting the fluorescence emission properties of the probe. Due to the varying number of negatively charged phosphate groups in ATP, ADP, and AMP (three, two, and one, respectively), it is feasible to design ATP probes with excellent selectivity based on electrostatic interactions.

In 2009, a pincer-like benzene-bridged probe **5** (Figure 3) was reported [4]. This probe utilized a pyrene excimer as the signal source and imidazolium as a phosphate anion receptor, enabling the detection of ATP. In probe **5**, the adenine moiety of ATP can be positioned between the two pyrene moieties, causing the separation of the pyrene moieties and the production of pyrene monomer fluorescence. However, other nucleoside triphosphates such as GTP, CTP, UTP, and TTP can only interact with the already stacked pyrene-pyrene dimer of probe **5** from the outside. This interaction results in the quenching of excimer fluorescence. In addition, probe **5** can distinguish ATP from ADP and AMP, which is attributed to the variation in electrostatic interactions between the probe and phosphate anion. Two years later, a tripodal probe **6** (Figure 3) featuring three naphthoimidazolium groups and three quaternary ammonium groups was developed. Probe **6** displays diverse interactions with different nucleoside bases, leading to varying synergistic effects of  $\pi$ -stacking and electrostatic interactions. Notably, probe **6** exhibits substantial fluorescence enhancements upon interaction with UTP, CTP, and TTP. It demonstrates moderate fluorescence enhancements when interacting with ATP and pyrophosphate. However, a fluorescence quenching effect is observed when probe **6** interacts with GTP. This distinct response to different nucleoside bases showcases the potential of probe **6** for selective detection and discrimination among nucleoside triphosphates [55].

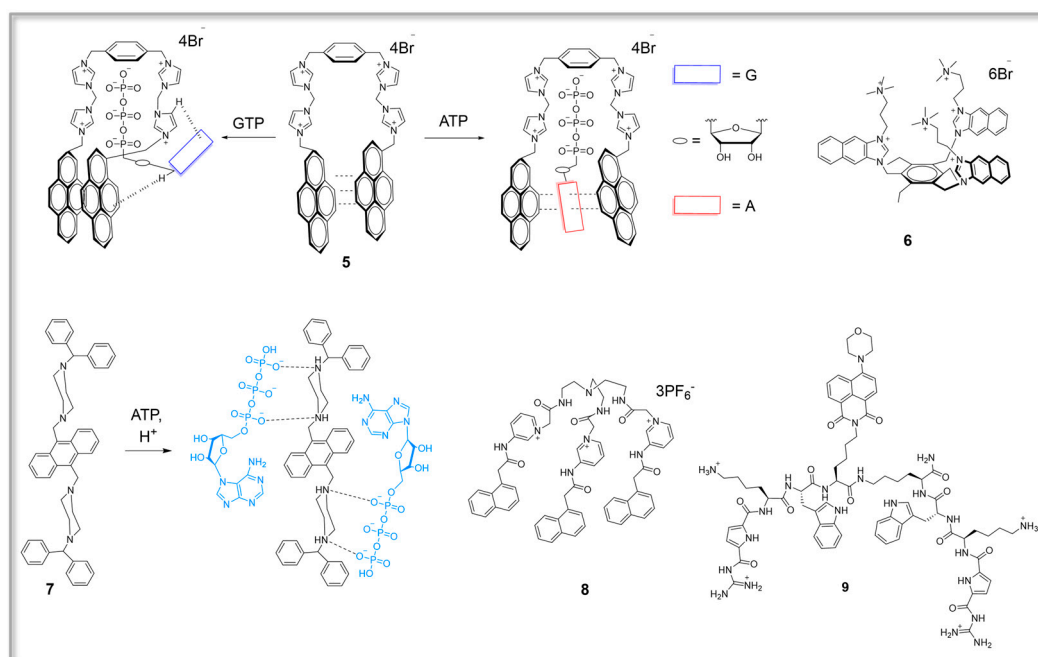


**Figure 3.** Structures and response mechanisms of fluorescent probes 5–9.

In 2015, a smart Off–On molecular scaffold/fluorescent probe **7** (Figure 3) was designed and synthesized [56]. The triphosphate unit of ATP interacts with the piperazine nitrogen atoms in probe **7** through hydrogen bonding and electrostatic interactions. These interactions synergistically enhance the CH– $\pi$  and  $\pi$ – $\pi$  stacking interactions between the anthracene and purine rings. As a result, a significantly enhanced “turn-on” emission is observed due to restricted photo-induced electron transfer (PET). Moreover, probe **7** exhibits outstanding photostability, cell permeability, organelle specificity, and remarkable selectivity for ATP. In the same year, a pyridinium-based probe **8** (Figure 3) was reported [57]. Probe **8** demonstrates the selective recognition of ATP by means of hydrogen bonding and electrostatic interactions at the pyridinium sites. Furthermore, probe **8** has been successfully used to detect intracellular ATP through fluorescent confocal imaging.

In 2016, fluorescence probe **9** (Figure 3) was reported [58]. Probe **9** consists of a naphthalimide fluorophore with two symmetric peptidic arms that incorporate a specifically designed anion-binding motif called guanidiniocarbonyl pyrrole. This motif enables the probe to selectively detect nucleoside triphosphates. The probe forms stable complexes with oxoanions through a salt bridge, reinforced by multiple hydrogen bonds. Each arm of the probe contains a lysine residue to facilitate additional electrostatic interactions. Moreover, the arms are functionalized with tryptophan, which has the potential to differentiate between nucleoside triphosphates based on their distinct  $\pi$ – $\pi$  interactions with the various nucleobases. The central spacer of probe **9** is linked to a green-emitting aminonaphthalimide fluorophore, serving as the reporter unit. Upon binding to nucleoside triphosphates, especially ATP, probe **9** exhibits a significant increase in fluorescence intensity, resulting in a prominent turn-on fluorescence response. The higher fluorescence intensity observed for triphosphates compared to diphosphates or monophosphates can be attributed to the differences in electrostatic interactions with the guanidiniocarbonyl pyrrole and lysine residues, which arise from the varying anionic charges of the different phosphate groups.

### 2.1.3. ATP Fluorescent Probes Based on Aggregation-Induced Emission

Conventional ATP sensors often face challenges related to emission quenching caused by the aggregation-induced quenching (ACQ) effect. Mitigating this quenching typically requires using low probe concentrations, which reduces the probe-to-analyte ratio and limits practical applications. However, the use of AIE luminogens (AIEgens) offers an

alternative approach. AIEgens are generally non-emissive or weakly emissive in their solution state but exhibit high emission intensity upon aggregation. This unique behavior of AIEgens effectively overcomes the fluorescence quenching issues observed with traditional fluorophores at high concentrations. At present, several AIE-based fluorescent probes for ATP detection have been reported, presenting promising solutions in the field.

In 2012, an ATP probe **10** (Figure 4) based on aggregation-induced luminescence was reported [59]. The interaction between the guanidinium and triphosphate groups plays a critical role in initiating the aggregation process, which ultimately leads to fluorescence enhancement. Additionally, the collective  $\pi$ - $\pi$  stacking and hydrophobic interactions with the adenine moiety contribute to the cooperative self-assembly phenomenon. These interactions result in nonlinear and substantial fluorescence enhancement, significantly improving the sensitivity and selectivity of the probe for ATP detection.

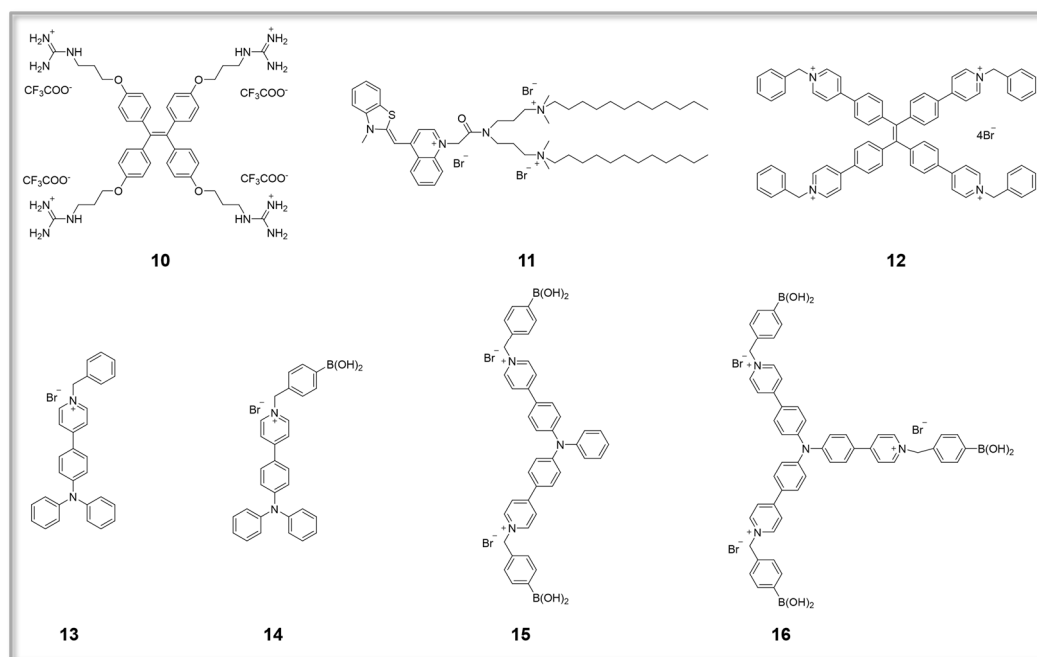


**Figure 4.** Structures of fluorescent probes **10**–**16**.

In 2015, a novel thiazole orange derivative **11** (Figure 4) was developed [60]. Probe **11** demonstrates cooperative co-assembly with ATP, leading to a nonlinear and responsive AIE signal. Upon the initial addition of ATP, a 1:2 complex of ATP/**11** is formed. At this stage, the dimer of probe **11** is relatively less stable, as it is modulated by only one ATP molecule, resulting in a slight enhancement of fluorescence. However, as more ATP is added, the preorganized 1:2 complexes of ATP/**11** promote the formation of higher-level complexes, such as extended “oligomer-” or “polymer-”like supramolecular arrays. Consequently, the dimer of probe **11** becomes more tightly packed and stable. This leads to a faster increase in intensity at 580 nm, being attributed to the intensified mutual interactions among the colocalized thiazole orange moieties of probe **11** within the assembly.

In 2017, an AIE-based tetraphenylethylene derivative (probe **12**, Figure 4) was developed for the fluorescence sensing of ATP in aqueous solution [61]. Probe **12**, featuring four cationic pyridinium pendants, exhibits weak emission in HEPES buffer solution. However, upon the addition of ATP, probe **12** undergoes aggregation along the ATP molecule through electrostatic interactions and hydrophobic interactions, resulting in a significant enhancement of emission. It is worth noting that probe **12** is capable of imaging ATP in both cancer cell lines and normal cell lines, demonstrating its potential as a versatile tool for ATP imaging.

In the same year, a series of novel AIE-active fluorescence probes (probe 13–16, Figure 4) were reported [62]. These probes incorporate pyridinium and boric acid groups and have been specifically designed for ATP recognition purposes. The unique design of these probes allows for two types of interaction modes and multiple connection sites with ATP molecules, enabling the selective discrimination of ATP from other bioactive anions. As a result, these probes exhibit a significant enhancement in fluorescence emission specifically upon ATP binding. Notably, probe 16, which incorporates two types of interaction modes and multiple connection sites, demonstrates high sensitivity in recognizing ATP. The above-described probes are summarized in Table 1.

**Table 1.** Summary of the ATP fluorescent probes based on organic small molecules in Section 2.1.

Probe	Fluorophore	$\lambda_{ex}/\lambda_{em}$ (nm)	Detection Type	ATP Detection Limit	ATP Detection Range (mM)	Analyte	Ref.
1	Rhodamine	520/583	Fluorescence enhancement	$2.5 \times 10^{-8}$ M	$1.0 \times 10^{-4}$ – $2.0 \times 10^{-1}$	ATP	[51]
2	Rhodamine, 1,8-naphthalimide	420/530, 580	Ratiometric	$1.0 \times 10^{-4}$ M	0–50	ATP	[52]
3	Rhodamine	500/560, 624	Ratiometric	Not determined	2.0–9.0	ATP	[53]
4	Rhodamine	660/700, 780	Ratiometric	Not determined	0–3.0	ATP, H <sup>+</sup>	[54]
5	Pyrene	345/375, 487	Ratiometric	Not determined	$0$ – $2.0 \times 10^{-1}$	ATP, GTP	[4]
6	Naphthoimidazolium	326/~460	Fluorescence enhancement	Not determined	$0$ – $6.0 \times 10^{-2}$	ATP, GTP	[55]
7	Piperazine–anthracene	376/402, 422	Fluorescence enhancement	$7 \times 10^{-6}$ M	$0$ – $1.0 \times 10^{-1}$	H <sup>+</sup> , ATP	[56]
8	Naphthalene	290/386	Fluorescence enhancement	$8.44 \times 10^{-6}$ M	$0$ – $1.0 \times 10^{-1}$	ATP	[57]
9	1,8-naphthalimide	410/540	Fluorescence enhancement	Not determined	$0$ – $1.4 \times 10^{-2}$	ATP	[58]
10	Tetraphenylethene	335/463	Fluorescence enhancement	Not determined	$0$ – $6.0 \times 10^{-2}$	ATP	[59]
11	Thiazole orange	520/580	Fluorescence enhancement	Not determined	$0$ – $8.0 \times 10^{-2}$	ATP	[60]
12	Tetraphenylethylene	365/500	Fluorescence enhancement	$7.5 \times 10^{-8}$ M	$1$ – $4.0 \times 10^{-3}$	ATP	[61]
13	Triphenylamine-pyridinium	427/613	Fluorescence enhancement	Not determined	$0$ – $3.0 \times 10^{-1}$	ATP	[62]
14	Triphenylamine-pyridinium	432/609	Fluorescence enhancement	Not determined	$0$ – $3.0 \times 10^{-1}$	ATP	[62]
15	Triphenylamine-pyridinium	437/614	Fluorescence enhancement	Not determined	$0$ – $3.0 \times 10^{-1}$	ATP	[62]
16	Triphenylamine-pyridinium	451/614	Fluorescence enhancement	0.3 ppm	$0$ – $3.0 \times 10^{-1}$	ATP	[62]

## 2.2. ATP Fluorescent Probes Based on Metal Complexes

Metal coordination complex-based fluorescent probes, characterized by one or two coordination sites, demonstrate a heightened affinity towards phosphate anions. This property makes them well-suited for the detection of ATP [63]. Fluorescent probes for ATP based on metal complexes have been widely studied in recent years due to their advantages of high selectivity, high sensitivity, and simple preparation.

### 2.2.1. ATP Fluorescent Probes Based on Zinc Complexes

Among the fluorescent probes based on metal complexes, zinc complexes have been rapidly developed. The Zn(II)-dipicolylamine (Zn-DPA) structural unit is widely used to design ATP fluorescent probes. The dipicolylamine unit can form a stable complex with Zn(II), and Zn(II) has a strong binding ability to the phosphate group of ATP. The change in the Zn(II) coordination unit after the addition of ATP causes a change in fluorescence. So far, Zn-DPA has been generally recognized as a specific recognition unit for ATP probes.

In 2002, fluorescent probe 17 (Figure 5) was developed. This probe incorporates an anthracene moiety appended with Zn-DPA, enabling efficient detection of ATP in a neutral aqueous solution. [64]. Probe 17 demonstrates a pronounced level of selectivity towards

ATP, as evidenced by the observed selectivity (ATP > ADP > AMP). This selectivity can be attributed to the disparities in the respective quantities of their anionic charges. After this study, a fluorescent chemosensor (probe **18**, Figure 5) for nucleoside polyphosphates such as ATP was reported in 2008 [65]. Probe **18** is designed with dual binding motifs, namely 2,2'-Dpa-Zn(II), and incorporates xanthene as a fluorescent sensing unit for nucleoside polyphosphates. The turn-on fluorescence sensing mechanism of probe **18** towards nucleoside polyphosphates can be attributed to the restoration of the conjugated structure of the xanthene ring. Initially, the fluorescence of probe **18** is suppressed due to the formation of a deconjugated structure in the xanthene fluorophore, as mentioned earlier. However, the binding of ATP to the two Zn(II)-Dpa sites disrupts the  $\mu$ -oxo-dizinc(II) core of probe **18** through multiple interactions with the triphosphate group of ATP. This disruption leads to the restoration of the conjugated xanthene structure and a significant increase in fluorescence emission. Importantly, probe **18** exhibits remarkable selectivity and sensitivity for ATP detection, making it highly suitable for visualizing ATP in living cells. In 2010, ratiometric probes **19** and **20** (Figure 5) for nucleoside polyphosphates such as ATP that are based on FRET combined with a turn-on fluorescence-sensing mechanism were developed [66]. In these probes, coumarin fluorophores were introduced as the FRET donors, and a binuclear zinc complex acted as the FRET acceptor. Probes **19** and **20** exhibited the distinct dual-emission signal change upon binding with high affinity ( $K_{app} \approx 10^6$ – $10^7$  M<sup>-1</sup>) to nucleoside polyphosphates in aqueous solutions. Notably, no significant emission changes were observed when these probes interacted with monophosphates, phosphodiester species, or various other anions.

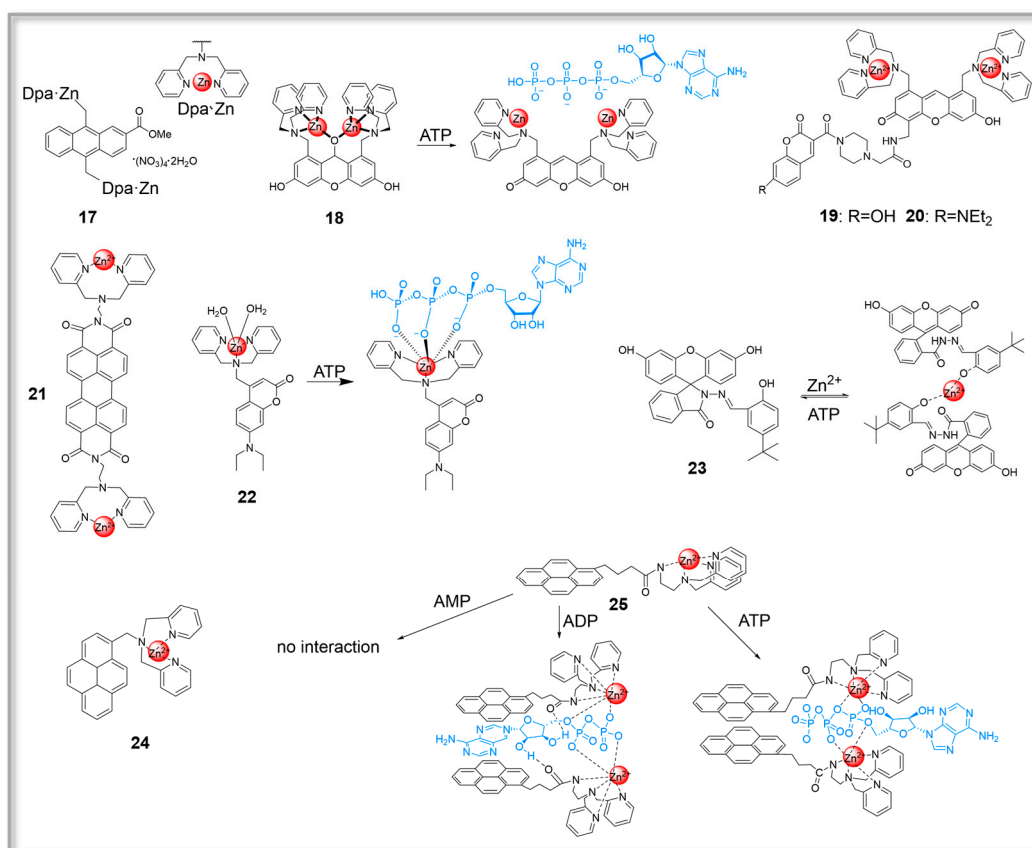


**Figure 5.** ATP fluorescent probes **17**–**25** based on zinc complexes.

In 2012, a perylene diimide (PDI) ligand (probe **21**, Figure 5) was developed, which was modified with a Zn<sup>2+</sup>-dipicolylethylenediamine (Zn<sup>2+</sup>-DPEN) moiety. This fluorometric chemosensor was developed with the specific aim of detecting ATP in aqueous solutions, demonstrating the selectivity over other phosphate anions. [67]. The binding stoichiometry

between probe **21** and ATP has been determined to be 1:1, indicating that one molecule of probe **21** interacts with one molecule of ATP. It is noteworthy that this probe displays high sensitivity and selectivity in detecting ATP, even in a 100% aqueous solution. In the presence of ATP, probe **21** exhibits a significant fluorescence enhancement, making it a reliable and effective tool for the detection of ATP.

In 2018, a coumarin and Zn(DPA)-based fluorescent probe **22** was reported [68]. As shown in Figure 5, the Zn(II) systems within the probe exhibit an affinity for ATP and ADP. The Zn(II) center of the Zn(DPA) moiety interacts with the pendent phosphate moieties of ATP and/or ADP. This binding event is expected to reduce the interaction between DPA moiety and Zn(II), leading to the weakening of the intramolecular charge transfer (ICT) process within the complex. As a result, the observed fluorescence intensity is enhanced.

In 2018, a reversible fluorescein-based fluorescent probe **23** for  $Zn^{2+}$  and ATP was designed and synthesized [69]. As shown in Figure 5, the sensing mechanism of probe **23** involves a fluorescence variation caused by the opening and closing of the spiro-ring of fluorescein. In its free form, the probe exhibits minimal emission due to the closed fluorescein spirolactam structure. However, upon the introduction of  $Zn^{2+}$ , a remarkable enhancement of fluorescence intensity at 527 nm is observed. This enhancement is attributed to the structural transformation induced by  $Zn^{2+}$ , leading to the conversion of the colorless spirolactam ring to the colored ring-opening delocalized form of fluorescein. Upon the gradual addition of ATP to a solution containing probe **23**- $Zn^{2+}$ , a significant decrease in fluorescence intensity at 527 nm is observed. This spectral change can be attributed to the strong binding affinity between ATP and  $Zn^{2+}$ . The binding of ATP to  $Zn^{2+}$  ions results in the displacement of  $Zn^{2+}$  from the complex, and the compound undergoes structural recovery. Upon the further addition of  $Zn^{2+}$ , the fluorescence is recovered, indicating the reversibility of the binding between probe **23** (**23**- $Zn^{2+}$ ) and  $Zn^{2+}$  (ATP).

$Zn^{2+}$  can combine with a variety of fluorophores to form a Zn-DPA structure for ATP detection. In 2012, a chemosensor (probe **24**, Figure 5) was synthesized based on a Zn complex of 1-[bis(pyridine-2-ylmethyl)amino]methylpyrene for the detection of nucleotides in aqueous solution [70]. Probe **24** exhibited a distinct emission band ranging from 360 to 450 nm, attributed to the emission from the pyrene monomer. Upon the addition of various nucleotide anions, the fluorescence intensity of the pyrene monomer emission noticeably increased upon the addition of PPI. By contrast, only a slight fluorescence enhancement was observed when ATP and ADP were added to the solution containing probe **24**. The spectra of other nucleotides displayed minimal changes, indicating limited interaction with the probe.

In 2014, a tailor-made ratiometric fluorescent probe **25** for nucleoside polyphosphates was fabricated based on a pyrene-functionalized zinc(II)-BPEA complex [71]. As shown in Figure 5, Probe **25** is composed of three components: a zinc(II)-BPEA complex (BPEA: *N,N*-bis(2-pyridylmethyl)ethylenediamine) serving as the ionophore, an amide residue acting as a hydrogen bond acceptor, and pyrene aromatic rings functioning as the fluorophore. These components synergistically form a fully intramolecular sandwich structure when two molecules of probe **25** interact with one molecule of ADP. This interaction is facilitated by three effects: (i) coordination of BPEA- $Zn^{2+}$  with the diphosphate anion; (ii) hydrogen bonding between the amide group and ribose; (iii)  $\pi$ - $\pi$  stacking interaction among the pyrene rings and adenine. By contrast, when two molecules of probe **25** interact with one molecule of ATP, a partial intramolecular sandwich structure is formed due to two synergistic interactions: coordination of BPEA- $Zn^{2+}$  with the triphosphate anion and  $\pi$ - $\pi$  stacking between the two pyrene rings. These distinctive binding patterns exhibited by probe **25** with ATP and ADP highlight its exceptional capability as a fluorescent probe for effectively distinguishing between ATP and ADP.

#### 2.2.2. ATP Fluorescent Probes Based on Copper Complexes

Although Zn(II) has a good recognition affinity for ATP, Cu(II) interacts more strongly with the phosphate moiety of ATP [72]. Several ATP fluorescent probes based on Cu(II)

complexes have been reported. In 2016, fluorescent probe **26** (Figure 6) with one 1,8-naphthalimide and two [12]aneN<sub>3</sub> units was reported [73]. Probe **26** exhibited strong fluorescence emission. However, in the presence of Cu<sup>2+</sup> ions, probe **26** formed a complex (**26**-Cu) with Cu<sup>2+</sup> ions in a 1:2 ratio, leading to a significant quenching of fluorescence emission. In the presence of ATP, a strong fluorescence enhancement was observed in the **26**-Cu complex. This enhancement can be attributed to the concerted coordination of the phosphates and adenosine base units of ATP to Cu(II) ions. This coordination effectively reduces the interaction between the Cu(II) ions and the amino group of the naphthalimide unit in probe **26**, resulting in the activation of its fluorescence. The coordinative interactions between copper(II) ions and adenosine play a crucial role in determining the selectivity of probe **26** [74–76]. When ADP is present, the diminished structure matching reduces the effectiveness of the interactions, resulting in reduced effects on the fluorescence response of probe **26**. On the other hand, the weak coordination of guanosine and thymidine base units to Cu<sup>2+</sup> ions leads to poor cooperative interactions between GTP/CTP and the **26**-Cu complex. As a result, there is almost no change observed in the fluorescent intensity when GTP or CTP is added to the system.

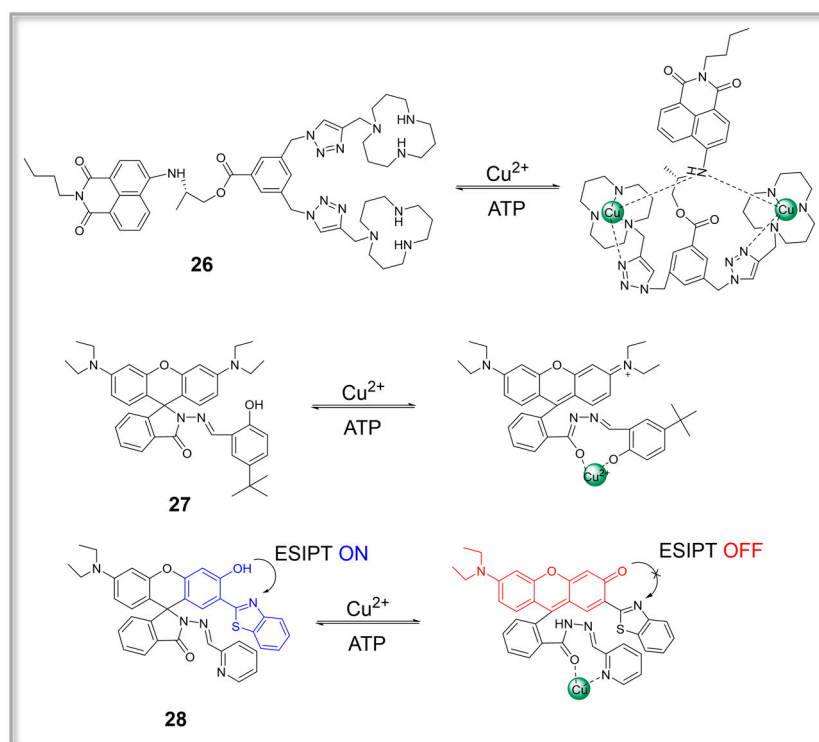


**Figure 6.** ATP fluorescent probes **26**–**28** based on copper complexes.

In 2018, a rhodamine-based fluorescent probe **27** (Figure 6) for Cu<sup>2+</sup> and ATP was reported [77]. Upon the addition of Cu<sup>2+</sup> ions, the fluorescence intensity or absorbance of the probe was significantly enhanced. This enhancement was attributed to the opening of the spiro-ring of the rhodamine moiety. However, the fluorescence or absorbance quickly returned to its original level as the probe underwent reconstruction upon reaction with ATP. The changes in fluorescence or absorbance induced by Cu<sup>2+</sup> and ATP exhibited a good linear relationship with the concentration of Cu<sup>2+</sup> ions in the range of 2–20 μM and ATP in the range of 0–10 μM. The detection limits for Cu<sup>2+</sup> and ATP were determined to be 0.1 μM and 1.0 μM, respectively.

In 2020, a rhodol-based ratiometric fluorescent probe **28** (Figure 6) was designed for the reversible response of Cu<sup>2+</sup> and ATP [78]. In the absence of Cu<sup>2+</sup>, probe **28** exhibits its maximal fluorescent intensity at 434 nm. This emission peak is attributed to the excited-state intramolecular proton transfer (ESIPT) process of the benzothiazole moiety present in

the probe. However, upon the addition of  $\text{Cu}^{2+}$ , the formation of the **28**–Cu complex occurs. As a result, the maximal emission peak at around 434 nm gradually diminishes, while a new emission intensity at around 595 nm significantly enhances. This new emission is characteristic of the opening ring of the rhodol spirolactam structure formed in the presence of  $\text{Cu}^{2+}$ . With the addition of ATP, free probe **28** is released from the **28**–Cu complex. The fluorescence of **28**–Cu gradually increased at 434 nm and decreased at 595 nm. Probe **28**/**28**–Cu can selectively respond to  $\text{Cu}^{2+}$ /ATP. Furthermore, the probe can be effectively utilized for the rapid and convenient detection of  $\text{Cu}^{2+}$  and ATP using filter paper and hydrogel as the detection platforms.

### 2.2.3. ATP Fluorescent Probes Based on Other Metal Complexes

In addition to  $\text{Zn}^{2+}$  and  $\text{Cu}^{2+}$ ,  $\text{Ga}^{3+}$  also has a strong binding affinity for diphosphate and triphosphate. Several ATP fluorescent probes based on gallium complexes have been reported. In 2014, a  $\text{Ga}^{3+}$  self-assembled fluorescent probe **29** (Figure 7) using the ligand of 2-(2',3'-dihydroxyphenyl)benzoxazole (DHBO) was synthesized [79]. The probe exhibits a significant fluorescence enhancement specifically with ATP among structurally similar nucleoside triphosphates under physiological conditions. The selectivity of probe **29** towards ATP can be attributed to several factors. First, ATP is attracted to probe **29** through electrostatic interactions between the positively charged  $\text{Ga}^{3+}$  ion and the phosphate group of ATP. The stronger the negative charge on the phosphate groups, the stronger the intermolecular interaction, which contributes to the selective recognition of ATP over ADP and AMP. Additionally, selective  $\pi$ – $\pi$  stacking interactions occur between the adenosine segment of ATP and DHBO ligand, further contributing to the sensing process. This  $\pi$ – $\pi$  stacking interaction is unique to ATP and not observed with other nucleoside triphosphates or pyrophosphate, providing additional selectivity for ATP. It is worth mentioning that probe **29** can also be employed for detecting the activity of ATP-related enzymes, further demonstrating its potential utility in enzyme activity assays and biological studies.

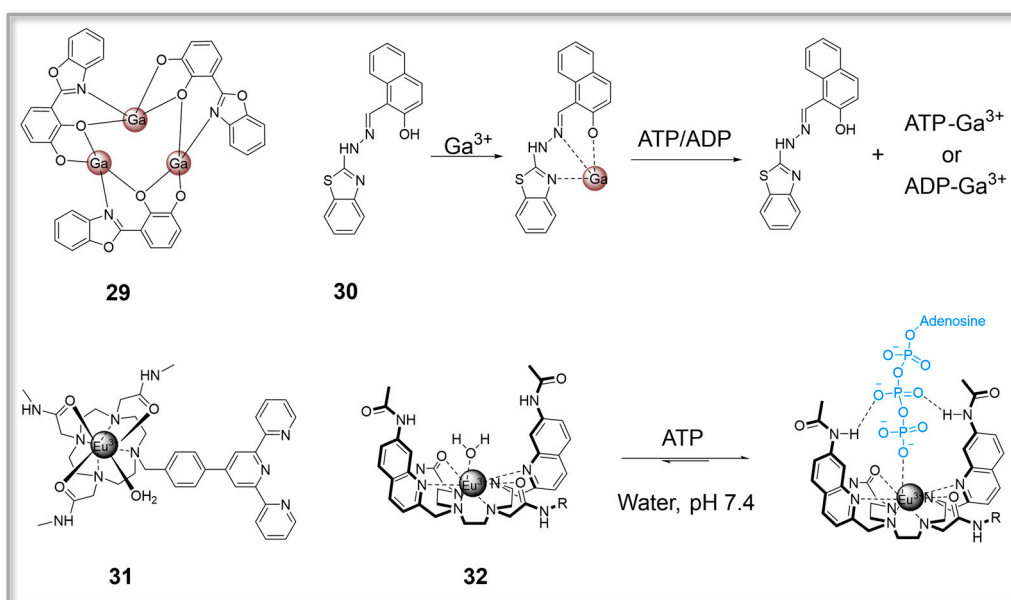


**Figure 7.** ATP fluorescent probes **29**–**32** based on other metal complexes.

In 2018, a naphthol-based fluorescent probe **30** (Figure 7) containing electron-donating Schiff base N, thiazole N, and phenolic OH, which provide binding sites to  $\text{Ga}^{3+}$ , was reported [80]. The fluorescence response of probe **30** to  $\text{Ga}^{3+}$  is based on a combination of two mechanisms: ESIPT and CHEF (chelation-enhanced fluorescence). Probe **30** exhibits a weak emission at 518 nm due to the presence of C=N and adjacent OH groups, which are characteristic of ESIPT. Upon the binding of  $\text{Ga}^{3+}$  to the C=N and OH groups, the ESIPT

process is further restrained. The formation of the stable complex  $30\text{-Ga}^{3+}$  leads to an enhanced fluorescence at 518 nm, attributed to the CHEF effect. The recognition of ATP by probe **30** involves the extrusion of  $\text{Ga}^{3+}$  from the  $30\text{-Ga}^{3+}$  complex, and this process is accompanied by ESIPT from the phenolic OH group to the Schiff base N in probe **30**. The combination of  $30\text{-Ga}^{3+}$  and ATP leads to the inhibition of CHEF and restoration of ESIPT, and thus the quenching of the bright green emission. Additionally, the  $30\text{-Ga}^{3+}$  complex exhibits high selectivity and sensitivity towards ADP and ATP over anions in aqueous solution. The presence of ADP and ATP in the solution displaces the  $\text{Ga}^{3+}$  from the complex, leading to quenching of the fluorescence. This selective recognition and quenching mechanism make the  $30\text{-Ga}^{3+}$  complex a suitable fluorescent probe for the detection of ADP and ATP.

Lanthanide complexes, particularly  $\text{Eu}^{3+}$  complexes, exhibit distinctive fluorescence responses in the recognition of ATP, demonstrating either a turn-on or turn-off behavior. Additionally, these complexes are known for their long fluorescence lifetimes. In 2013, fluorescent probe **31** (Figure 7) based on a  $\text{Eu}^{3+}$  complex was developed [81]. This probe demonstrates excellent selectivity, allowing for the effective differentiation of ATP from ADP and AMP in an aqueous solution at pH 6.8. The proposed mechanism for the enhancement of luminescence can be described as follows: First, the terpyridine arm chain of the ligand is well-suited for ATP, facilitating coordinated interactions and  $\pi\text{-}\pi$  stacking interactions with the probe. Second, the  $\pi\text{-}\pi$  stacking interactions between the terpyridine group of the ligand and ATP contribute to the reinforcement of the conjugate planes' rigidity within the antenna groups. This interaction also restricts the rotation of C-C bonds between the aromatic rings. Additionally, compared with probes based on organic molecules and transition metal complexes, lanthanide-based probe **31** offers the advantage of an extended fluorescence lifetime.

In 2018, fluorescent probe **32** (Figure 7) based on a luminescent lanthanide complex was reported [82]. Probe **32**, which contains two neutral amide donors, demonstrates a strong binding affinity towards ATP ( $\log K_a = 5.8$ ). This binding interaction leads to the formation of a stable ternary complex. Notably, the resulting ternary complex exhibits intense and long-lived luminescence attributed to the presence of  $\text{Eu}^{3+}$ . Furthermore, in a competitive aqueous medium that mimics the intricate ionic environment found in cells, probe **32** displays effective discrimination between ATP, ADP, and AMP. The above-described probes are summarized in Table 2.

**Table 2.** Summary of the ATP fluorescent probes based on metal complexes in Section 2.2.

Probe	Fluorophore	$\lambda_{\text{ex}}/\lambda_{\text{em}}$ (nm)	Detection Type	ATP Detection Limit	ATP Detection Range (mM)	Analyte	Ref.
17	Anthracene	380/460	Fluorescence enhancement	Not determined	$0\text{-}1.8 \times 10^{-2}$	ATP	[64]
18	Xanthene	488/522	Fluorescence enhancement	$1.0 \times 10^{-6}$ M	$0\text{-}1.0 \times 10^{-2}$	ATP	[65]
19	Xanthene, coumarin	341/454, 525	Ratiometric	Not determined	$0\text{-}5.0 \times 10^{-3}$	[ATP], [ATP] + [ADP]	[66]
20	Xanthene, coumarin	414/477, 525	Ratiometric	Not determined	$0\text{-}5.0 \times 10^{-3}$	[ATP], [ATP] + [ADP]	[66]
21	Perylene diimide	500/559	Fluorescence enhancement	Not determined	$0\text{-}1.0 \times 10^{-1}$	ATP	[67]
22	Coumarin	400/500	Fluorescence enhancement	$8.4 \times 10^{-9}$ M	$0\text{-}5.0 \times 10^{-3}$	ATP	[68]
23	Fluorescein	420/527	Fluorescence quenching	$5.0 \times 10^{-7}$ M	$0\text{-}1.0 \times 10^{-2}$	ATP, $\text{Zn}^{2+}$	[69]
24	Pyrene	346/383	Fluorescence enhancement	Not determined	$1.0 \times 10^{-1}$	Nucleotides	[70]
25	Pyrene	350/390, 482	Ratiometric	Not determined	$0\text{-}3.0 \times 10^{-2}$	ATP, ADP, AMP	[71]
26	1,8-naphthalimide	451/541	Fluorescence enhancement	$8.5 \times 10^{-9}$ M	$0\text{-}1.0 \times 10^{-1}$	ATP, $\text{Cu}^{2+}$	[73]
27	Rhodamine	510/575	Fluorescence quenching	$1.0 \times 10^{-6}$ M	$0\text{-}1.0 \times 10^{-2}$	ATP, $\text{Cu}^{2+}$	[77]
28	Benzothiazole, xanthenes	380/434, 595	Ratiometric	$8.0 \times 10^{-8}$ M	$0\text{-}1.0 \times 10^{-2}$	ATP, $\text{Cu}^{2+}$	[78]

Table 2. Cont.

Probe	Fluorophore	$\lambda_{ex}/\lambda_{em}$ (nm)	Detection Type	ATP Detection Limit	ATP Detection Range (mM)	Analyte	Ref.
29	2-(2',3'-dihydroxyphenyl) benzoxazole-Ga <sup>3+</sup> complex	360/461	Fluorescence enhancement	$5.49 \times 10^{-7}$ M	$1.0 \times 10^{-3}$ – $1.0 \times 10^{-2}$	ATP, Ga <sup>3+</sup>	[79]
30	Naphthol-Ga <sup>3+</sup> complex	440/518	Fluorescence quenching	Not determined	$0$ – $2.75 \times 10^{-2}$	Ga <sup>3+</sup> , ATP, ADP	[80]
31	Eu <sup>3+</sup>	335/591, 615	Fluorescence enhancement	$8.87 \times 10^{-6}$ M	$0$ – $2.5 \times 10^{-2}$	ATP	[81]
32	Eu <sup>3+</sup>	330/688, 697	Fluorescence enhancement	Not determined	$0$ – $3.0$	ATP	[82]

### 2.3. ATP Fluorescent Probes Based on Water-Soluble Conjugated Polymers

Water-soluble conjugated polymers have broad application prospects in the field of chemical and biological sensing [83]. The molecule of this polymer can linearly amplify the fluorescence signal to detect various analytes with high sensitivity.

In 2004, a water-soluble cationic polythiophene derivative **33** (Figure 8) was reported [84]. The probe exhibits both colorimetric and fluorescent responses to ATP. The response mechanism involves a combination of electrostatic and hydrophobic interactions. The interaction between the negatively charged triphosphate group of ATP and the positively charged ammonium group in **33** facilitates the planarization of the polythiophene backbone. As the concentration of ATP increases, a critical threshold is reached, promoting efficient  $\pi$ – $\pi$  stacking interactions between the backbones of probe **33**. These stacking interactions are induced by the synergistic effect of hydrophobic interactions between the adenine units. Consequently, these interactions cause a shift in the  $\pi$ – $\pi^*$  transition to longer wavelengths, leading to a color change from yellow to pink-red. Additionally, the fluorescence of probe **33** is quenched because of the interactions with ATP.

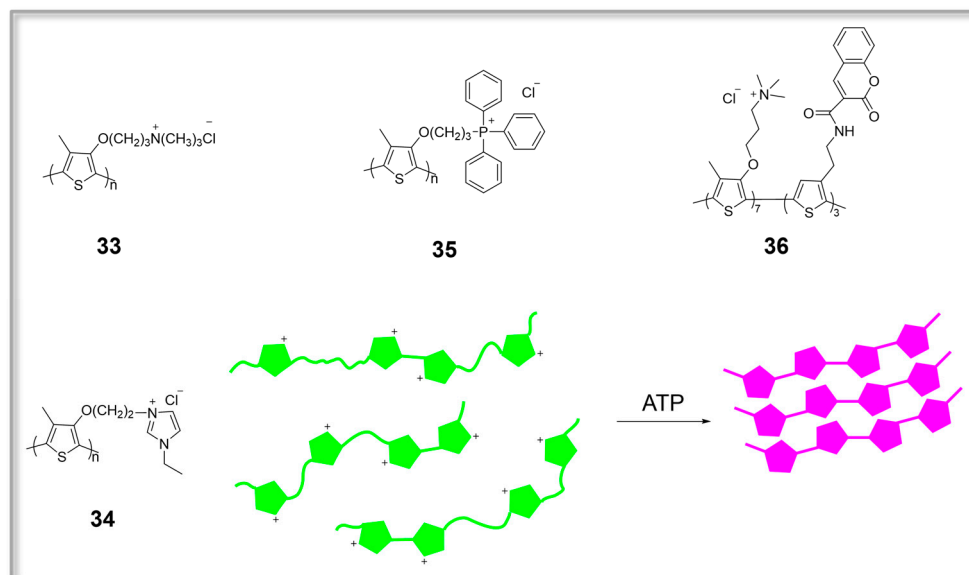


Figure 8. ATP fluorescent probes **33**–**36** based on water-soluble conjugated polymers.

In 2016, a new water-soluble cationic polythiophene derivative **34** (Figure 8) was developed as a specific fluorescent probe for detecting ATP [85]. Probe **34** demonstrates a random coil conformation in water, but it undergoes conformational changes and forms aggregates upon interacting with ATP. The presence of ATP induces the aggregation of isolated probe **34** through cooperative electrostatic and hydrophobic interactions. Consequently, this conformational transition from a random coil structure to aggregates leads to the simultaneous quenching of probe **34**'s fluorescence. In 2017, another water-soluble cationic polythiophene derivative (probe **35**, Figure 8) for ATP sensing was reported [86].

In an aqueous solution, probe **35** adopts a random coil conformation. When it is exposed to ATP, probe **35** undergoes electrostatic and hydrophobic interactions, leading to its aggregation. This conformational transition from a random coil structure to aggregates results in the quenching of the probe's fluorescence. Notably, probe **35** displays excellent sensitivity and selectivity towards ATP.

In 2017, a ratiometric probe **36** (Figure 8) for the detection of ATP was reported [87]. This probe utilizes a sensing mechanism that combines binding-induced modulation of FRET with aggregation-caused quenching (ACQ). To develop the ratiometric probe **36**, coumarin fluorophores are introduced as the FRET donors into the side chain of polythiophene, which serves as the FRET acceptor. Upon the addition of ATP, the polymer/ATP complex is formed, resulting in conformational changes of the polythiophene backbone from a random coil structure to a planar conformation, along with aggregation. By exploiting the changes in spectral overlap before and after the addition of ATP, the ratiometric detection of ATP can be achieved by modulating the FRET efficiency between the coumarin fluorophores and the polythiophene backbone, coupled with ACQ. Importantly, probe **36** demonstrates a distinct dual-emission signal change resembling a seesaw type upon binding to ATP in an aqueous solution, exhibiting a strong affinity ( $K_{app} = 3.12 \times 10^4 \text{ M}^{-1}$ ). Notably, no significant emission changes are observed with ADP, AMP, or various other anions, highlighting the high selectivity of probe **36** towards ATP. The above-described probes are summarized in Table 3.

**Table 3.** Summary of the ATP fluorescent probes based on water-soluble conjugated polymers in Section 2.3.

Probe	Fluorophore	$\lambda_{ex}/\lambda_{em}$ (nm)	Detection Type	ATP Detection Limit	ATP Detection Range (mM)	Analyte	Ref.
<b>33</b>	Polythiophene	445/529	Fluorescence quenching	$1.0 \times 10^{-8} \text{ M}$	$0-5 \times 10^{-1}$	ATP	[84]
<b>34</b>	Polythiophene	410/520	Fluorescence quenching	$3.6 \times 10^{-11} \text{ M}$	$0-7.5 \times 10^{-4}$	ATP	[85]
<b>35</b>	Polythiophene	410/524	Fluorescence quenching	$2.7 \times 10^{-8} \text{ M}$	$0-2.5 \times 10^{-3}$	ATP	[86]
<b>36</b>	Polythiophene, coumarin	300/410, 568	Ratiometric	$2.9 \times 10^{-8} \text{ M}$	$0-2.8 \times 10^{-2}$	ATP	[87]

### 3. Imaging Applications of ATP Fluorescent Probes

In recent years, ATP fluorescent probes have made significant progress. Some ATP probes can sensitively detect the content, distribution, and dynamic changes in ATP in cells. Organelle-targeted ATP probes can accurately detect ATP in specific organelles, which helps to deepen the understanding of organelle function. Some ATP fluorescent probes can also be used to visualize the process of cellular biological events. In addition, some probes can be used for imaging changes in ATP content in diseases, which is expected to provide new tools for the diagnosis of related diseases.

#### 3.1. ATP Fluorescent Probes for Targeting Organelles

ATP plays an important role in various life activities within cells, so it is necessary to detect ATP in specific cells or organelles. Fluorescent probes targeting cells and organelles have been a research hotspot, and ATP-based targeted fluorescent probes have also been widely studied. Among various organelles, mitochondria are the major sites of ATP production. In 2017, a fluorescent probe named **37** (Figure 9) was synthesized and used to recognize ATP in mitochondria [88]. Rhodamine, diethylenetriamine, and triphenylphosphonium were chosen as the fluorophore, reaction site, and mitochondria-targeting group, respectively. Probe **37** exhibited remarkable sensitivity to ATP. The detection range (0.1–10 mM) of the probe effectively matched the concentration levels of ATP found within the mitochondria. Notably, probe **37** exhibited exceptional selectivity towards ATP compared with other biological anions, thanks to the synergistic effect of its dual recognition sites. Additionally, this probe demonstrated specific localization within the mitochondria and proved to be a valuable tool for the real-time monitoring of changes in mitochondrial ATP concentration.

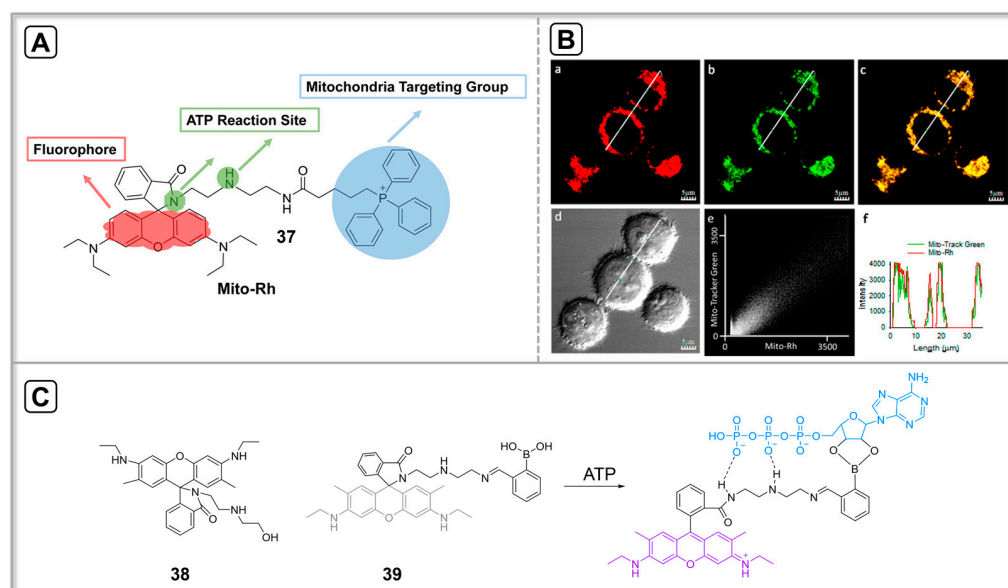


**Figure 9.** (A) Chemical structure of probe 37. (B) Colocalization imaging of HeLa cells staining with probe 37 and MitoTracker Green. (a) The cells were stained with probe 37 (1  $\mu$ M) in the red channel. (b) The cells were stained with MitoTracker Green (1  $\mu$ M) in the green channel. (c) Merged image. (d) Bright-field image. (e) Intensity scatter plot of probe 37 and MitoTracker Green. (f) Fluorescence intensity profile of regions of interest (white line in parts (a,b)). Scale bar, 5  $\mu$ m. Reprinted with permission from [88]. Copyright 2017, American Chemical Society. (C) Mitochondria-targeting ATP fluorescent probes 38–39.

In 2017, a novel fluorescent probe 38 (Figure 9) was designed as a colorimetric and fluorescent chemosensor for ATP detection based on hydrogen bond interactions [89]. The probe exhibited a significant “turn-on” fluorescence response upon ATP binding, with a 15-fold increase in fluorescence intensity observed upon the addition of 10 equivalents of ATP. To further investigate its potential applications, colocalization experiments were conducted using MitoTracker Green, confirming the selective imaging capability of probe 38 within the mitochondria.

In 2018, a multisite-binding fluorescent probe 39 (Figure 9) for ATP was reported [90]. The fluorophore, reaction sites, and mitochondria-targeting group chosen for the design of probe 39 were rhodamine 6G, diethylenetriamine (or phenylboronic acid), and phenylboronic acid, respectively. Notably, probe 39 demonstrated excellent selectivity towards ATP, surpassing other anions, thanks to the synergistic effect of its multisite-binding recognition. Live-cell imaging experiments revealed that probe 39 exhibited preferential localization within the mitochondria maintaining good biocompatibility. Furthermore, the probe proved to be a valuable tool for real-time monitoring of changes in mitochondrial ATP concentration.

Lysosomes in cells can stimulate ATP production through  $\text{Ca}^{2+}$ -dependent exocytosis [91], so it becomes crucial to monitor ATP levels specifically within lysosomes to gain insights into the cellular ATP dynamics and its role in various cellular processes. In 2019, a NIR fluorescent probe 40 (Figure 10) for targeting lysosomes and detecting ATP in cells was designed [92]. Probe 40, initially in a non-fluorescent closed form, exhibited a remarkable increase in fluorescence intensity upon exposure to ATP. The interaction between ATP and the probe was facilitated by the formation of hydrogen bonds between the ATP phosphate group and the diethylenetriamine moiety of the probe, along with a  $\pi$ - $\pi$  stacking interaction between the adenine group and the xanthene moiety. Furthermore, the presence of the morpholine moiety in probe 40 conferred specificity towards lysosomes. When cells were stained with probe 40, red fluorescence was observed in the red channel, while the cells stained with lysotracker blue displayed blue fluorescence. The red fluorescent signal from

probe **40** and the blue fluorescence from the lysotracker showed significant overlap, as indicated by a Pearson's coefficient of 0.78. This overlap confirms that probe **40** primarily localizes within the lysosomes. Additionally, probe **40** demonstrated high photostability, making it suitable for long-term monitoring of ATP levels in lysosomes.

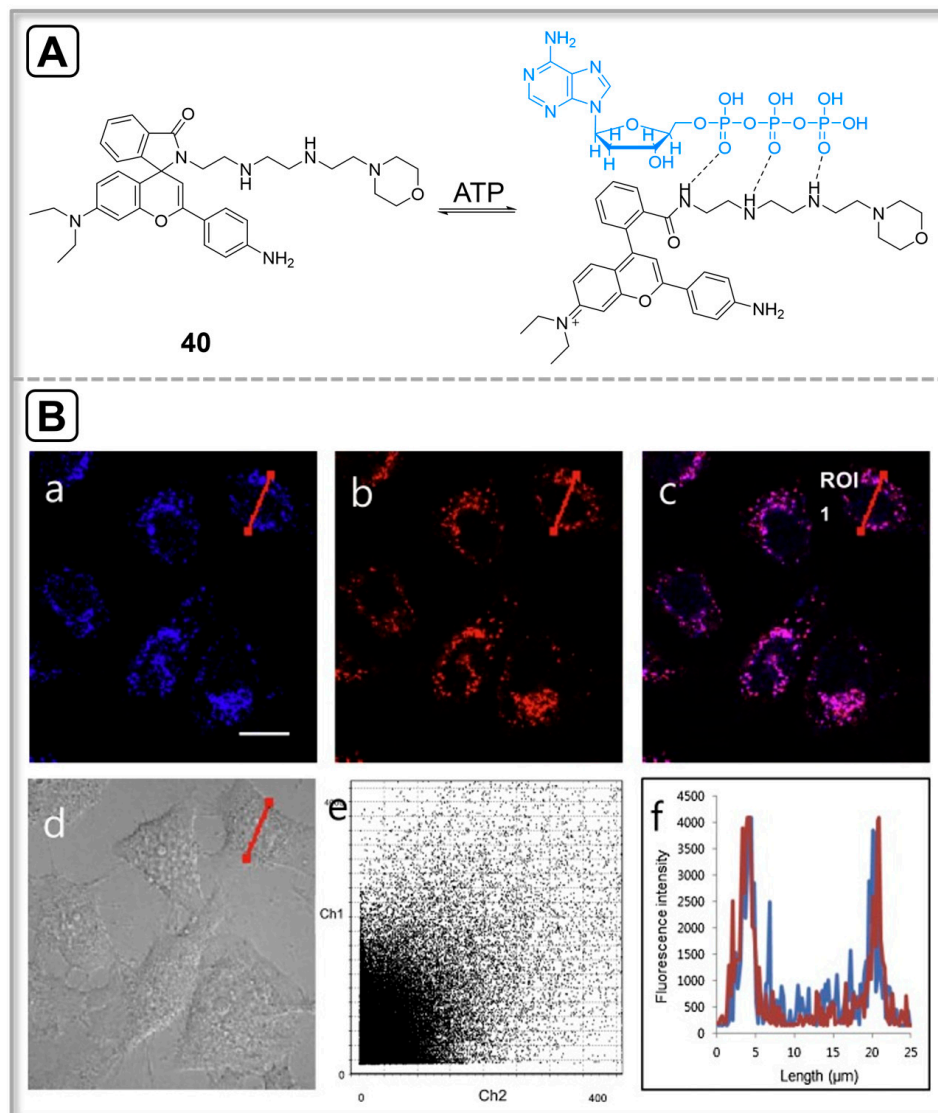


**Figure 10.** (A) Lysosomes targeting ATP fluorescent probe **40**. (B) HeLa cells were co-stained with 20  $\mu$ M probe **40** and 200 nM Lysotracker Blue DND-22 for 30 min and fluorescence images were acquired by confocal microscopy. (a) Lysotracker Blue DND-22, (b) probe **40**, (c) merged image, (d) DIC image, (e) co-localization analysis graph of Lysotracker and probe **40** (Ch 1: Lysotracker; Ch 2: probe **40**), (f) Fluorescence intensity profile of ROI (region of interest) shown in (d) image: blue line, Lysotracker; red line, probe **40**. Scale bar: 20  $\mu$ m. Reprinted with permission from [92]. Copyright 2019, Elsevier.

The significant role of ATP in the nucleus, acting as a hydrotrope and chelator of free  $Mg^{2+}$  ions, contributes to the solubilization of chromatin and nuclear macromolecules [93]. As a result, the development of a small-molecule probe capable of tracking and imaging nuclear ATP holds unique value, enabling a better understanding of its dynamics and functions within this specific cellular compartment. In 2023, probe **41** (Figure 11) was developed, which exhibits selective detection of nuclear ATP through reversible binding [94]. The Zn(II) complex probe **41** exhibits minimal fluorescence in pH 7.4 HEPES buffer. However,

in the presence of ATP, probe **41** undergoes a significant fluorescence enhancement. The probe's fluorescence signal shows a high degree of overlap with that of a nucleus tracker, Nuclear-ID Red, as evidenced by a high Pearson's colocalization coefficient (PCC = 0.89). This indicates the probe's ability to accurately localize within the nucleus. In addition, probe **41** demonstrates the potential to differentiate between tumor tissues and normal tissues, as well as cancer cells and normal cells, based on the varying levels of nuclear ATP. Using this probe, significantly higher nuclear ATP levels are observed in cancerous cell lines (2.1–3.3-fold higher) and tumor tissues (3.9–7.8-fold higher) compared to normal cell lines and tissues, respectively.

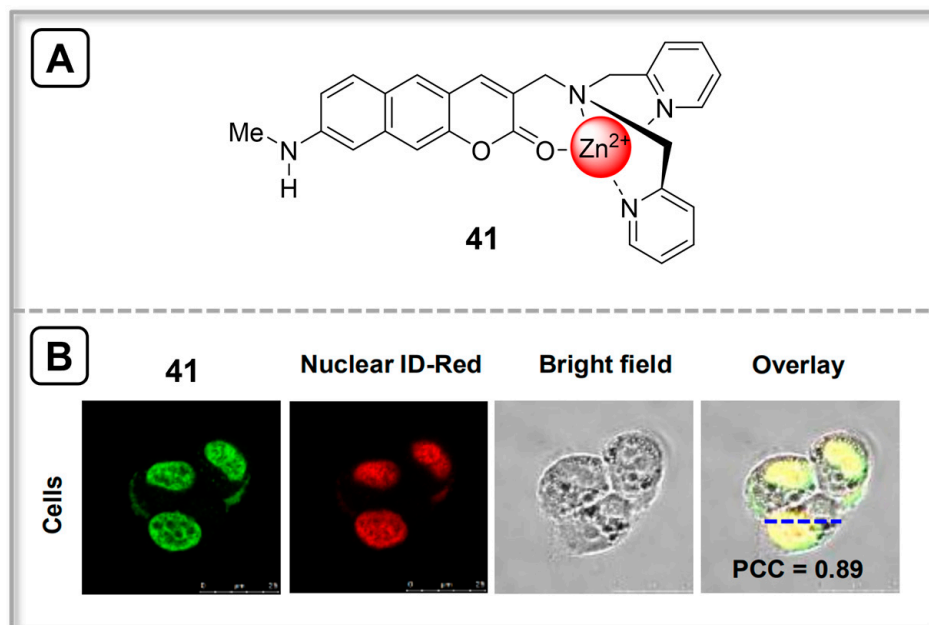


**Figure 11.** (A) Nucleus-targeting ATP fluorescent probe **41**. (B) Colocalization imaging of PC3 cells stained with probe **41** and Nuclear-ID Red. Reprinted with permission from [94]. Copyright 2023, Wiley-VCH.

Cell membranes serve as protective barriers for the cytoplasm of living cells and are crucial for energy production [95]. The detection of ATP within the cell membrane is of critical importance. By understanding the levels and dynamics of membrane ATP, researchers can gain a better understanding of cellular energy metabolism, signaling pathways, and the overall functioning of the plasma membrane in different biological contexts. In 2012, fluorescent probes **42** and **43** (Figure 12) that detect the dynamics of NPPs in specific regions of living cells were reported [96]. Both probes, probe **42** and rhodamine-type complex **43**, are functionalized as turn-on-type fluorescent probes specifically designed for ATP detection. In live cell imaging experiments, probe **42**, which incorporates a lipid anchor, selectively localizes to the surface of the plasma membrane. On the other hand, probe **43** spontaneously localizes within the mitochondria of cells. Through the simultaneous use of probes **42** and **43**, multicolor images can be obtained, enabling the detection of ATP dynamics within different cellular compartments simultaneously. Probes **42** and **43** have been employed to monitor changes in ATP levels concurrently on the plasma membrane surface and within the mitochondria of HeLa cells treated with KCN (an inhibitor of oxidative phosphorylation).

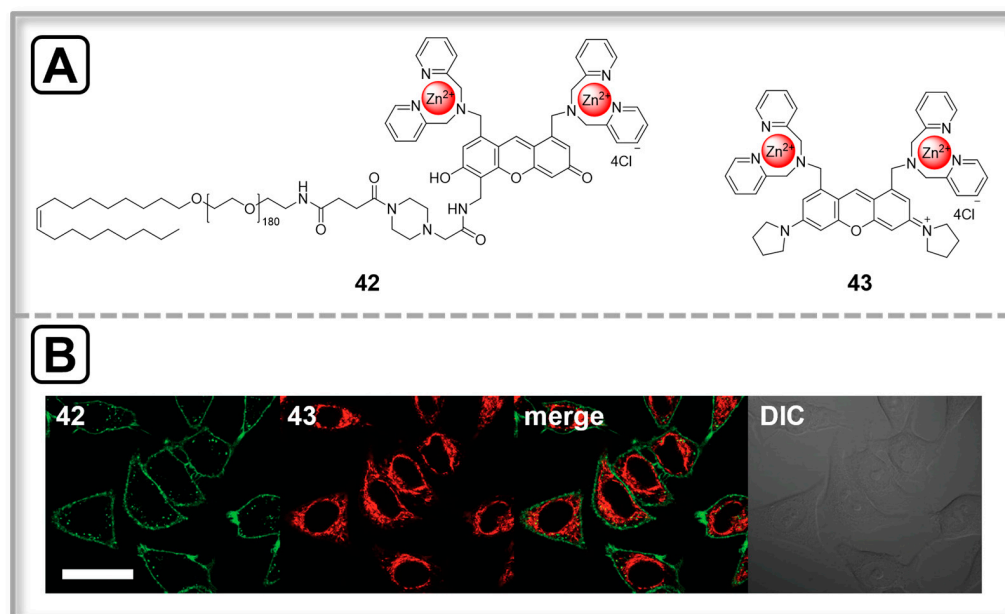


**Figure 12.** (A) Structures of ATP fluorescent probes **42** and **43**. (B) Confocal micrographs of HeLa cells stained with probes **42** and **43**. Scale bars: 20  $\mu\text{m}$ . Reprinted with permission from [96]. Copyright 2012, American Chemical Society.

### 3.2. ATP Fluorescent Probes for the Imaging of Cell Biological Events

ATP and its derivatives (NPPs) are related to many cell biological events. Tracking the change of ATP content in cellular biological events is helpful in understanding the cellular life process. The use of ATP fluorescent probes to track cell life activities has been a hot topic of research. Vesicles, which are small compartments bound by lipid bilayers, play a crucial role in the secretion and uptake of cellular substances through membrane fusion processes. These membrane fusion processes are vital in various biological events, including viral infection, fertilization, and the release of neurotransmitters and hormones into the extracellular environment through exocytosis [97,98]. In 2018, a ratiometric two-photon ATP probe **44** (Figure 13) was reported, which enables the direct monitoring of membrane fusion processes between vesicles, specifically lysosomes [99]. This probe not only provides qualitative visual information but also offers quantitative data regarding ATP levels involved in the fusion processes. Probe **44** exhibits ATP sensing capabilities specifically in the acidic pH range of lysosomes, rather than the cytosolic pH range. The application of probe **44** in live-cell imaging experiments has enabled the direct visualization of the lysosomal membrane fusion process in cells. The results show that the kiss-and-run process involves repeated transient interactions between lysosomes, allowing for gradual content mixing. By contrast, the full fusion process occurs in a single event. Importantly, it is confirmed that both fusion processes maintain the conservation of the content present within the lysosomes.

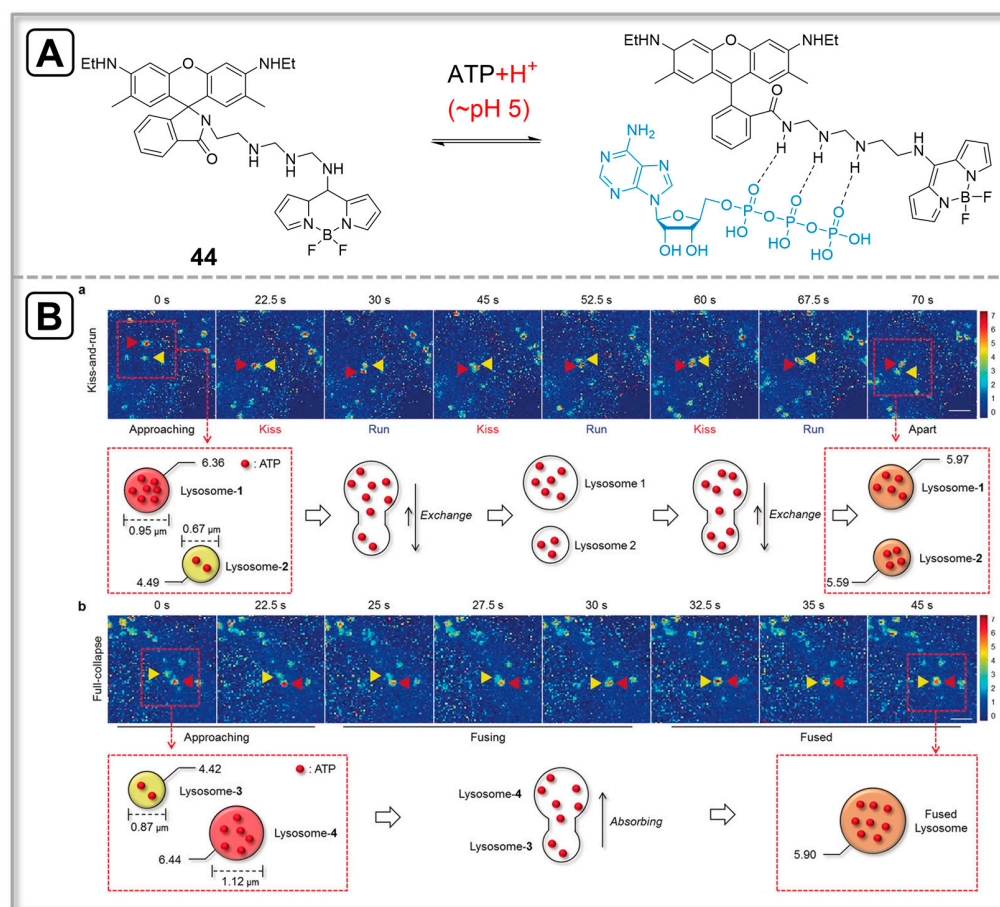


**Figure 13.** (A) Mechanism of reaction between probe **44** and ATP. (B) Two-photon live-cell images of lysosomes that undergo (a) ‘kiss-and-run’ and (b) ‘full-collapse fusion’ processes, processed with pixel-to-pixel ratio images containing the quantitative information on ATP, and schematics of the two processes. HeLa cells incubated with probe **44** (10 μM) were used. The values indicate the emission intensity ratio values ( $I_{\text{Yellow}}/I_{\text{Blue}}$ ). Scale bar = 7.5 μm (a,b). Reprinted with permission from [99]. Copyright 2018, Wiley-VCH.

Hypoxia, a common characteristic of solid tumors, arises due to insufficient blood flow and serves as a critical indicator for various medical conditions including cancer, stroke, ischemia, and cardiovascular diseases [100]. Existing evidence suggests that hypoxic cells have the propensity to upregulate the expression of nitroreductase (NTR) [101]. Nitroreductases are capable of reducing nitroaromatic compounds to their corresponding amines in the presence of reduced nicotinamide adenine dinucleotide (NADH). In 2018, a dual-function fluorescent probe **45** (Figure 14) for detecting nitroreductase (NTR) and ATP with different responses was developed [102]. Probe **45** was developed using a rhodamine/1,8-naphthalimide hybrid structure as the platform. The probe incorporates a nitro group as the reaction site for nitroreductase (NTR) and diethylenetriamine as the reaction site for ATP. This design allows probe **45** to interact with NTR, ATP, and NTR/ATP, resulting in distinct fluorescence responses. Furthermore, through cell imaging studies using probe **45**, it has been observed that ATP serves as a hypoxia-sensitive species. During the hypoxic process, intracellular NTR and ATP display contrasting changes. NTR demonstrates an approximately exponential increase, while ATP shows a decrease. This inverse relationship between NTR and ATP levels can effectively indicate the degree of hypoxia in living cells.

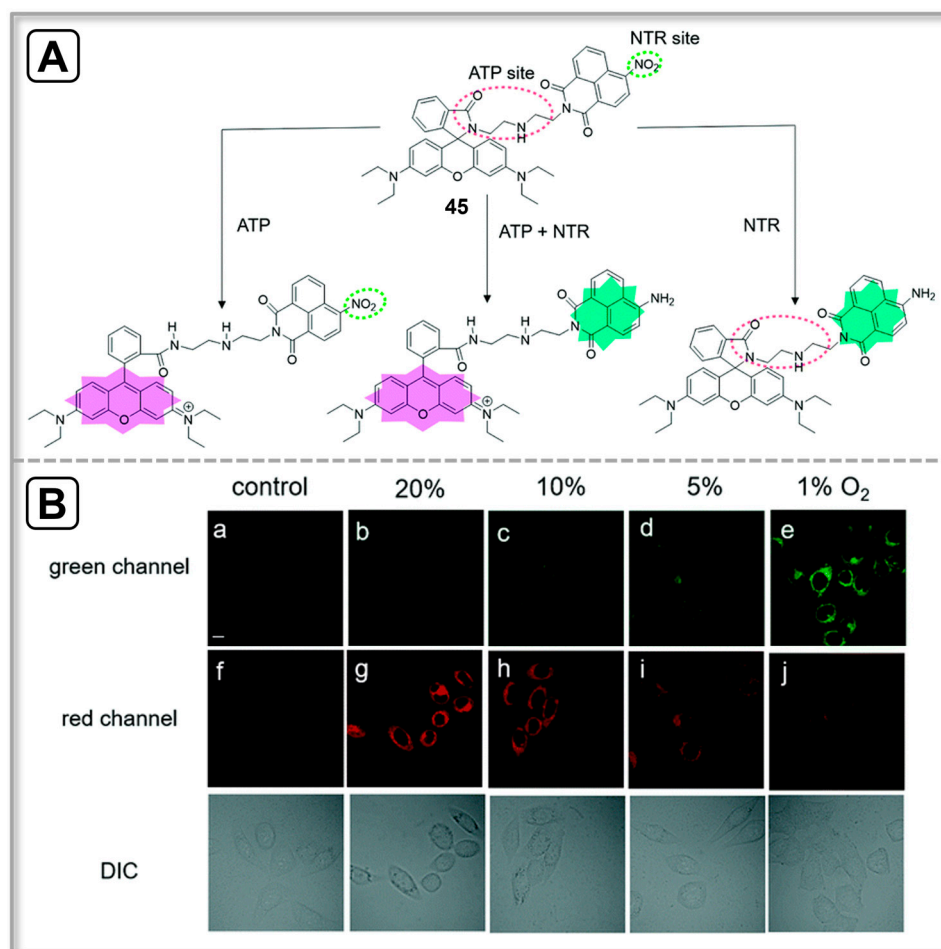


**Figure 14.** (A) Structure of ATP fluorescent probe 45. (B) Confocal fluorescence images of HeLa cells under normoxic (20% O<sub>2</sub>) and different degrees of hypoxic conditions (10%, 5%, and 1%). Control (HeLa cells themselves); the cells were grown and then incubated with 10 mM probe 45 for 40 min at different O<sub>2</sub> concentrations; green channel for NTR and red channel for ATP. Scale bar: 10 μm. Reprinted with permission from [102]. Copyright 2018, Royal Society of Chemistry.

Mitochondrial oxidative stress and energy metabolism play crucial roles in various physiological and pathological processes, including apoptosis and necrosis. One key component involved in maintaining mitochondrial redox processes and signaling mitochondrial damage is H<sub>2</sub>O<sub>2</sub> [103,104]. Furthermore, adenosine triphosphate (ATP) acts as another important messenger in regulating mitochondrial energy metabolism [105,106]. In 2020, a single two-photon fluorescence-lifetime-based probe 46 (Figure 15) that enabled real-time imaging and simultaneous determination of mitochondrial H<sub>2</sub>O<sub>2</sub> and ATP changes in distinct fluorescence channels without spectral crosstalk, was reported [107]. The positively charged nature of probe 46 facilitated its remarkable targeting of mitochondria. This probe was utilized to investigate the relationship between H<sub>2</sub>O<sub>2</sub> and ATP in mitochondria and visualize the dynamic changes in their levels induced by the superoxide anion (O<sub>2</sub><sup>•−</sup>). The researchers discovered that short-term stimulation with O<sub>2</sub><sup>•−</sup> (8 min) transiently altered the levels of H<sub>2</sub>O<sub>2</sub> and ATP in mitochondria, with neurons being capable of recovering to their initial state within a brief period. However, prolonged exposure to O<sub>2</sub><sup>•−</sup> for up to 50 min resulted in permanent oxidative damage and energy deficiency. Furthermore, it was revealed that exogenous stimulation with O<sub>2</sub><sup>•−</sup> and H<sub>2</sub>O<sub>2</sub> had distinct impacts on the levels of mitochondrial H<sub>2</sub>O<sub>2</sub> and ATP, with O<sub>2</sub><sup>•−</sup> demonstrating more severe and negative consequences. This study not only provided a general molecular design methodology for imaging multiple species but also shed light on the intracellular functions related to H<sub>2</sub>O<sub>2</sub>

and ATP in mitochondria in response to oxidative stress, based on the developed probe **46**. It contributes to the deep understanding of the complex interplay between  $\text{H}_2\text{O}_2$ , ATP, and oxidative stress within the mitochondria.

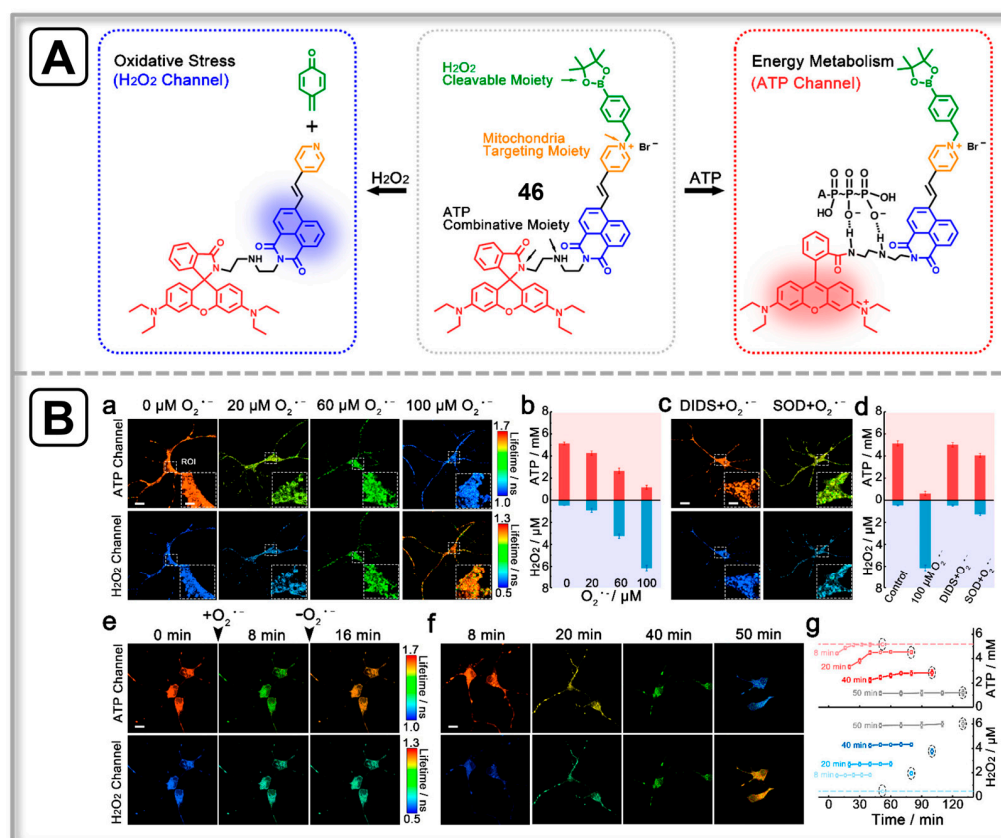


**Figure 15.** (A) The response mechanism of probe **46**. (B) Fluorescence imaging and simultaneous quantification of mitochondrial  $\text{H}_2\text{O}_2$  and ATP in response to exogenous  $\text{O}_2^{\bullet-}$  stimulation. (a) Fluorescence lifetime images of neurons under  $\text{O}_2^{\bullet-}$  stimulation. (b) Summarized data of mitochondrial levels of  $\text{H}_2\text{O}_2$  and ATP in (a). (c) Fluorescence lifetime images of neurons after being treated with  $\text{O}_2^{\bullet-}$  in the presence of DIDS or SOD. Scale bars: 10  $\mu\text{m}$  for the whole images and 2  $\mu\text{m}$  for ROI images. (d) Summarized data of  $\text{H}_2\text{O}_2$  and ATP changes in (c). (e) Fluorescence lifetime images of neurons stimulated with  $\text{O}_2^{\bullet-}$  for 8 min in the incubation of **46** (10  $\mu\text{M}$ ) at different times. Scale bar: 6  $\mu\text{m}$ . (f) Fluorescence lifetime images of neurons stimulated with  $\text{O}_2^{\bullet-}$  (100  $\mu\text{M}$ ) after 8, 20, 40, and 50 min. Scale bar: 6  $\mu\text{m}$ . (g) Summarized data of mitochondrial  $\text{H}_2\text{O}_2$  and ATP changes under  $\text{O}_2^{\bullet-}$  stimulation at different times. The circled data represent the final levels in each stimulation, and the cyan and red dotted lines represent the initial levels of  $\text{H}_2\text{O}_2$  and ATP, respectively. Error bars: SD,  $n = 8$ . Reprinted with permission from [107]. Copyright 2020, American Chemical Society.

### 3.3. ATP Fluorescent Probes for the Imaging of Disease Markers

The development of some diseases (such as drug-induced liver injury and cancer) can cause changes in ATP levels. Therefore, ATP can be used as a biomarker for some diseases. Currently, the application of ATP fluorescent probes in disease detection is a research hotspot. Peroxynitrite ( $\text{ONOO}^-$ ) is a reactive nitrogen species (RNS). It is known to inhibit ATP production by oxidatively deactivating mitochondrial ATP synthase [108]. In various pathological events, correlations between ATP and peroxynitrite concentrations have been observed. [109,110]. In 2021, fluorescent probe **47** (Figure 16) was reported, which enables the simultaneous detection of  $\text{ONOO}^-$  and ATP [111]. Probe **47** is designed to detect both peroxynitrite ( $\text{ONOO}^-$ ) and ATP through distinct fluorescence responses. The boronate pinacol ester of probe **47** undergoes selective oxidation by  $\text{ONOO}^-$ , leading to the formation of a fluorescent 4-hydroxy-1,8-naphthalimide product. On the other hand, ATP

binding to probe **47** triggers the opening of the spirolactam ring of rhodamine, resulting in the generation of a highly emissive product. By utilizing probe **47** and two different fluorescence channels, it becomes possible to simultaneously monitor the enhancement of  $\text{ONOO}^-$  and the depletion of ATP during acetaminophen (APAP)-induced hepatotoxicity. This monitoring approach provides support for the proposed signaling pathways associated with APAP-induced liver toxicity. It is believed that the increase in  $\text{ONOO}^-$  levels and the depletion of ATP play crucial roles in the development of hepatic necrosis [112].

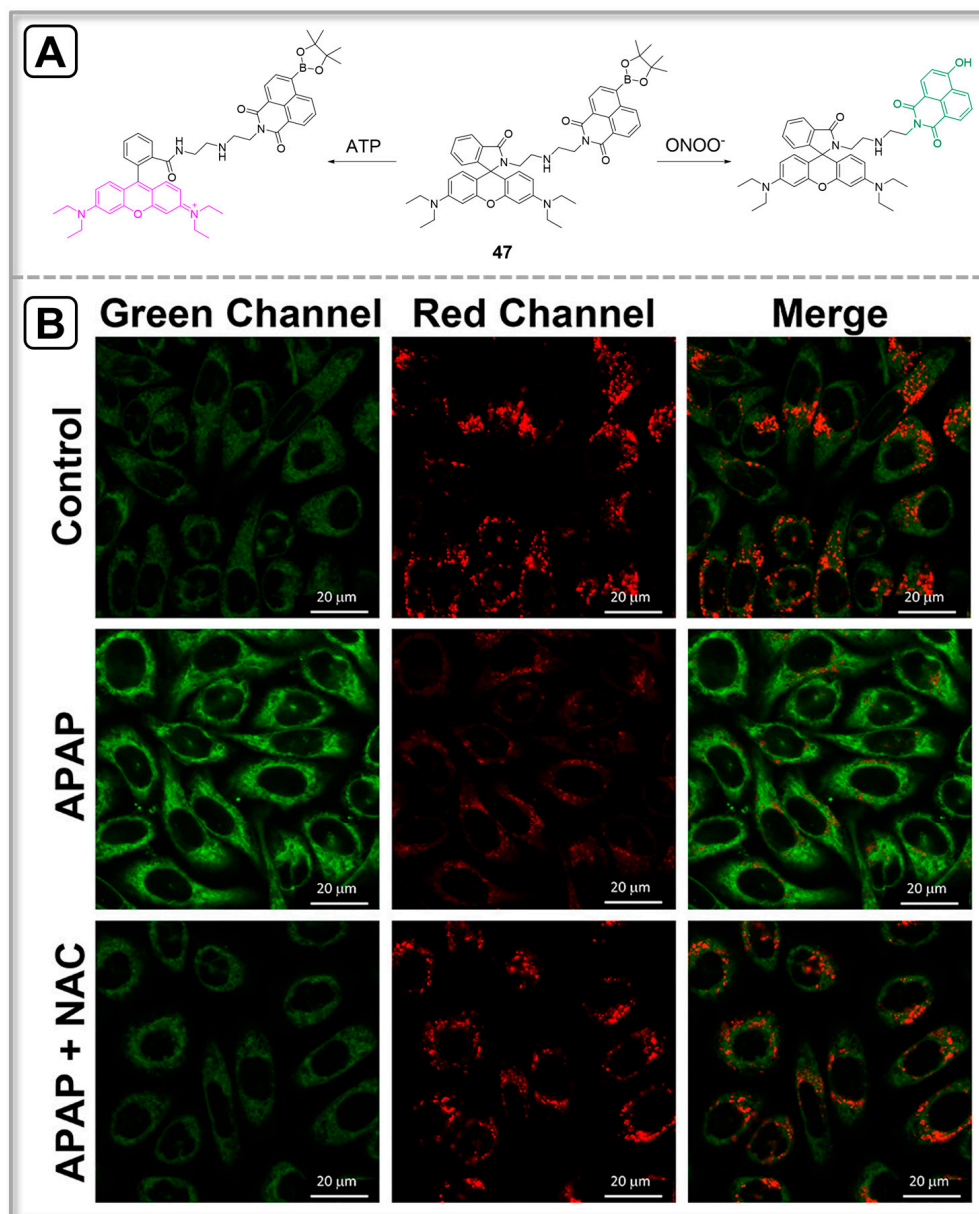


**Figure 16.** (A) response mechanism of dual-analyte fluorescent probe **47**. (B) Confocal images of APAP-induced liver injury and its remediation by NAC in HL-7702 cells. Green channel for  $\text{ONOO}^-$  and red channel for ATP. Reprinted with permission from [111]. Copyright 2021, American Chemical Society.

Clinical data suggest that cancer cells exhibit increased glucose metabolism, a phenomenon known as the Warburg effect. As a result, it has been observed that the endogenous ATP concentration in cancer cells is generally higher compared to normal cells. In 2022, a tumor-targeting NIR fluorescent probe **48** (Figure 17) was developed for ATP detection in tumor cells and tissues [113]. Probe **48** consists of three main components:

a si-rhodamine-based fluorophore, a diethylenetriamine-based recognition group, and a biotin-based tumor-targetable group. When probe **48** interacts with ATP, a significant increase in fluorescence emission at 675 nm is observed, making it suitable for *in vivo* applications in mice. One of the key advantages of probe **48** is its excellent selectivity for ATP over other potential biological analytes. The dual recognition sites present in the probe contribute to this high selectivity. Furthermore, probe **48** is equipped with a biotin-based tumor-targetable group. This enables the probe to selectively accumulate in cancer cells, guided by the presence of biotin receptors on the cell surface. As a result, probe **48** exhibits a strong fluorescence response to ATP specifically in cancer cells. It is worth noting that compared to contrast probe **49**, which lacks the biotin-based tumor-targetable group, probe **48** demonstrates a higher signal-to-noise ratio and a stronger fluorescence signal for tumor imaging. This enhanced performance of probe **48** makes it a promising tool for elucidating the role of ATP in clinical cancer diagnosis. The above-described probes are summarized in Table 4.

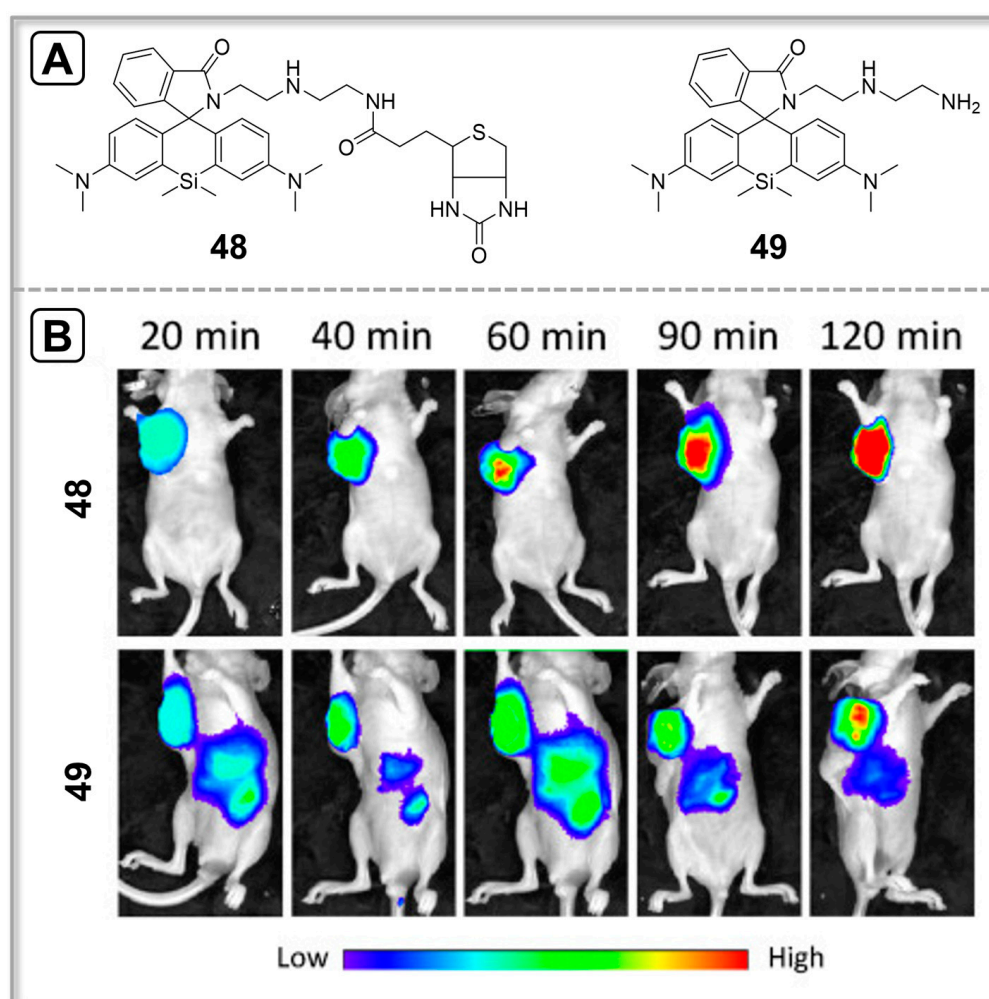


**Figure 17.** (A) Chemical structures of probes **48** and **49**. (B) Fluorescence imaging of tumor-bearing mice. The mice were given an intravenous injection of **48** or **49** at different times. Reprinted with permission from [113]. Copyright 2022, Elsevier.

**Table 4.** Summary of the imaging applications of ATP fluorescent probes in Section 3.

Probe	Fluorophore	$\lambda_{ex}/\lambda_{em}$ (nm)	Detection Type	Application	Targeting	Analyte	Ref.
37	Rhodamine	520/583	Fluorescence enhancement	Cell imaging	Mitochondria-targeting	ATP	[88]
38	Rhodamine	527/557	Fluorescence enhancement	Cell imaging	Mitochondria-targeting	ATP	[89]
39	Rhodamine	510/558	Fluorescence enhancement	Cell imaging	Mitochondria-targeting	ATP	[90]
40	Rhodamine	480/634	Fluorescence enhancement	Cell imaging	Lysosome-targeting	ATP	[92]
41	Benzocoumarin	400/595	Fluorescence enhancement	Cell imaging	Nucleus-targeting	ATP	[94]
42	Xanthene	450/528	Fluorescence enhancement	Cell imaging	Plasma-membrane-surface-targeting	ATP	[96]
43	Xanthene	543/590	Fluorescence enhancement	Cell imaging	Mitochondria-targeting	ATP	[96]
44	Rhodamine, BODIPY	403/454, 557	Ratiometric	Cell imaging	Lysosome-targeting	ATP, H <sup>+</sup>	[99]
45	Rhodamine	540/580	Fluorescence enhancement	Cell imaging	NO	NTR, ATP	[102]
46	Rhodamine	710/590	Fluorescence enhancement	Cell imaging, Zebrafish imaging	Mitochondria-targeting	H <sub>2</sub> O <sub>2</sub> , ATP	[107]
47	Rhodamine	520/587	Fluorescence enhancement	Cell imaging	NO	ATP, ONOO <sup>-</sup>	[111]
48	Rhodamine	640/675	Fluorescence enhancement	Cell imaging, Mice imaging	Tumor-targeting	ATP	[113]
49	Rhodamine	Not determined	Fluorescence enhancement	Cell imaging, Mice imaging	NO	ATP	[113]

#### 4. Summary and Outlook

In this review, we discuss recent advances in the detection of ATP *in vitro* and *in vivo* based on fluorescent probes. The design strategies of ATP fluorescent probes are divided into three categories, which are based on organic small molecules, metal complexes, and water-soluble conjugated polymers. These probes mainly contain organic fluorophores and ATP recognition sites, among which the recognition sites can interact with ATP to cause changes in fluorophore structure or energy transfer, thus causing changes in fluorescence signals. This paper also focuses on the application of ATP fluorescence probes in the imaging of targeted organelles, cell biological events, and disease markers. Although many ATP fluorescence probes have been developed, there are still challenges in the application of ATP fluorescence probes in cells and *in vivo*. The following are our views on these challenges and prospects for the development of ATP fluorescent probes: (1) The excitation wavelength and emission wavelength of most existing ATP fluorescence probes are in the visible region, which makes them difficult to be applied in *in vivo* imaging. NIR-I and NIR-II fluorescent probes have longer excitation and emission wavelengths, thus increasing the penetration depth in biological samples and reducing the interference of spontaneous fluorescence. Therefore, it is of great significance to develop long-wavelength ATP fluorescent probes. (2) Cell life activities are often involved in a variety of bioactive substances, and it is difficult to accurately monitor such biological events with a single fluorescent probe for ATP detection. The development of fluorescent probes that simultaneously image ATP and other related signaling molecules can provide more information about relevant life activities, which is conducive to a comprehensive and accurate understanding of complex cell biological events. (3) Photoacoustic imaging uses ultrasonic waves as the photoacoustic signal and its low scattering property allows it to obtain good spatial resolution in deep tissue. The development of probes with both fluorescence and photoacoustic dual-mode imaging performance can complement the advantages of fluorescence imaging's high sensitivity and photoacoustic imaging's tissue penetration ability to better detect ATP *in vivo*.

**Author Contributions:** Conceptualization, Q.-S.G.; writing—original draft preparation, Q.-S.G., T.L. (Ting Li), T.L. (Ting Liu), G.Y., G.-J.M. and F.X.; project administration, writing—review and editing, C.-Y.L. All authors have read and agreed to the published version of the manuscript.

**Funding:** This work was supported by the National Natural Science Foundation of China (22174122, 21775133), the Hunan Provincial Natural Science Foundation (2021JJ30654), the Scientific Research Fund of the Hunan Provincial Education Department (19A479), the Open Research Fund of the School of Chemistry and Chemical Engineering, Henan Normal University (2020YB01), the Key Science Research Project of Higher Education of the Henan Province (23A150016), and the Hunan Provincial Innovation Foundation for Postgraduates (CX20220593).

**Institutional Review Board Statement:** Not applicable.

**Informed Consent Statement:** Not applicable.

**Data Availability Statement:** Not applicable.

**Conflicts of Interest:** The authors declare no conflict of interest.

## References

1. Patel, A.; Malinowska, L.; Saha, S.; Wang, J.; Alberti, S.; Krishnan, Y.; Hyman, A.A. ATP as a biological hydrotrope. *Science* **2017**, *356*, 753–756. [[CrossRef](#)] [[PubMed](#)]
2. Fields, R.D.; Stevens, B. ATP: An extracellular signaling molecule between neurons and glia. *Trends Neurosci.* **2000**, *23*, 625–633. [[CrossRef](#)] [[PubMed](#)]
3. Shen, X.; Mizuguchi, G.; Hamiche, A.; Wu, C. A chromatin remodelling complex involved in transcription and DNA processing. *Nature* **2000**, *406*, 541–544. [[CrossRef](#)]
4. Xu, Z.; Singh, N.J.; Lim, J.; Pan, J.; Kim, H.N.; Park, S.; Kim, K.S.; Yoon, J. Unique sandwich stacking of pyrene-adenine-pyrene for selective and ratiometric fluorescent sensing of ATP at physiological pH. *J. Am. Chem. Soc.* **2009**, *131*, 15528–15533. [[CrossRef](#)] [[PubMed](#)]
5. Impellizzeri, F.M.; Marcora, S.M.; Castagna, C.; Reilly, T.; Sassi, A.; Iaia, F.M.; Rampinini, E. Physiological and performance effects of generic versus specific aerobic training in soccer players. *Int. J. Sports Med.* **2006**, *27*, 483–492. [[CrossRef](#)]
6. Dennis, P.B.; Jaeschke, A.; Saitoh, M.; Fowler, B.; Kozma, S.C.; Thomas, G. Mammalian TOR: A homeostatic ATP sensor. *Science* **2001**, *294*, 1102–1105. [[CrossRef](#)]
7. Ashcroft, F.M.; Gribble, F.M. ATP-sensitive K<sup>+</sup> channels and insulin secretion: Their role in health and disease. *Diabetologia* **1999**, *42*, 903–919. [[CrossRef](#)]
8. Van Wylen, D.G.; Park, T.S.; Rubio, R.; Berne, R.M. Increases in cerebral interstitial fluid adenosine concentration during hypoxia, local potassium infusion, and ischemia. *J. Cereb. Blood Flow Metab.* **1986**, *6*, 522–528. [[CrossRef](#)]
9. Zhu, C.; Zhao, Y.; Yan, M.; Huang, Y.; Yan, J.; Bai, W.; Chen, A. A sandwich dipstick assay for ATP detection based on split aptamer fragments. *Anal. Bioanal. Chem.* **2016**, *408*, 4151–4158. [[CrossRef](#)]
10. Sweeney, M.I. Neuroprotective effects of adenosine in cerebral ischemia: Window of opportunity. *Neurosci. Biobehav. Rev.* **1997**, *21*, 207–217. [[CrossRef](#)]
11. Bush, K.T.; Keller, S.H.; Nigam, S.K. Genesis and reversal of the ischemic phenotype in epithelial cells. *J. Clin. Investig.* **2000**, *106*, 621–626. [[CrossRef](#)] [[PubMed](#)]
12. Makela, A.; Kuusi, T.; Schroder, T. Inhibition of serum phospholipase-A2 in acute pancreatitis by pharmacological agents in vitro. *Scand. J. Clin. Lab. Investig.* **1997**, *57*, 401–407. [[CrossRef](#)] [[PubMed](#)]
13. Cruz-Aguado, J.A.; Chen, Y.; Zhang, Z.; Elowe, N.H.; Brook, M.A.; Brennan, J.D. Ultrasensitive ATP Detection Using Firefly Luciferase Entrapped in Sugar-Modified Sol–Gel-Derived Silica. *J. Am. Chem. Soc.* **2004**, *126*, 6878–6879. [[CrossRef](#)] [[PubMed](#)]
14. Yu, P.; He, X.; Zhang, L.; Mao, L. Dual recognition unit strategy improves the specificity of the adenosine triphosphate (ATP) aptamer biosensor for cerebral ATP assay. *Anal. Chem.* **2015**, *87*, 1373–1380. [[CrossRef](#)] [[PubMed](#)]
15. Huang, Y.F.; Chang, H.T. Analysis of adenosine triphosphate and glutathione through gold nanoparticles assisted laser desorption/ionization mass spectrometry. *Anal. Chem.* **2007**, *79*, 4852–4859. [[CrossRef](#)]
16. Xie, P.J.; Ye, M.L.; Hu, Z.Y.; Pan, G.W.; Zhu, Y.; Zhang, J.J. Determination of levels of adenosine phosphates in blood by ion chromatography. *Chin. Chem. Lett.* **2011**, *22*, 1485–1488. [[CrossRef](#)]
17. Mora, L.; Hernandez-Cazares, A.S.; Aristoy, M.C.; Toldra, F. Hydrophilic interaction chromatographic determination of adenosine triphosphate and its metabolites. *Food Chem.* **2010**, *123*, 1282–1288. [[CrossRef](#)]
18. Yang, Y.M.; Zhao, Q.; Feng, W.; Li, F.Y. Luminescent chemodosimeters for bioimaging. *Chem. Rev.* **2013**, *113*, 192–270. [[CrossRef](#)]
19. Li, X.; Gao, X.; Shi, W.; Ma, H. Design strategies for water-soluble small molecular chromogenic and fluorogenic probes. *Chem. Rev.* **2014**, *114*, 590–659. [[CrossRef](#)]
20. Li, Z.; Liang, T.; Lv, S.W.; Zhuang, Q.G.; Liu, Z.H. A Rationally Designed Upconversion Nanoprobe for in Vivo Detection of Hydroxyl Radical. *J. Am. Chem. Soc.* **2015**, *137*, 11179–11185. [[CrossRef](#)]

21. Wu, F.; Liu, J.; Tao, M.; Wang, M.; Ren, X.; Hai, Z.  $\beta$ -Galactosidase-Activatable Fluorescent and Photoacoustic Imaging of Tumor Senescence. *Anal. Chem.* **2023**, *95*, 10481–10485. [[CrossRef](#)] [[PubMed](#)]
22. Liu, Y.; Zhou, J.; Wang, L.L.; Hu, X.X.; Liu, X.J.; Liu, M.R.; Cao, Z.H.; Shangguan, D.H.; Tan, W.H. A Cyanine Dye to Probe Mitophagy: Simultaneous Detection of Mitochondria and Autolysosomes in Live Cells. *J. Am. Chem. Soc.* **2016**, *138*, 12368–12374. [[CrossRef](#)] [[PubMed](#)]
23. Zhang, X.F.; Wang, B.L.; Wang, C.; Chen, L.C.; Xiao, Y. Monitoring Lipid Peroxidation within Foam Cells by Lysosome-Targetable and Ratiometric Probe. *Anal. Chem.* **2015**, *87*, 8292–8300. [[CrossRef](#)]
24. Mao, Z.Q.; Feng, W.Q.; Li, Z.; Zeng, L.Y.; Lv, W.J.; Liu, Z.H. NIR in, far-red out: Developing a two-photon fluorescent probe for tracking nitric oxide in deep tissue. *Chem. Sci.* **2016**, *7*, 5230–5235. [[CrossRef](#)]
25. Liu, Y.C.; Teng, L.L.; Chen, L.L.; Ma, H.C.; Liu, H.W.; Zhang, X.B. Engineering of a near-infrared fluorescent probe for real-time simultaneous visualization of intracellular hypoxia and induced mitophagy. *Chem. Sci.* **2018**, *9*, 5347–5353. [[CrossRef](#)]
26. Zhu, B.C.; Li, P.; Shu, W.; Wang, X.; Liu, C.Y.; Wang, Y.; Wang, Z.K.; Wang, Y.W.; Tang, B. Highly Specific and Ultrasensitive Two-Photon Fluorescence Imaging of Native HOCl in Lysosomes and Tissues Based on Thiocarbamate Derivatives. *Anal. Chem.* **2016**, *88*, 12532–12538. [[CrossRef](#)]
27. Gao, S.T.; Tang, G.S.; Hua, D.W.; Xiong, R.H.; Han, J.Q.; Jiang, S.H.; Zhang, Q.L.; Huang, C.B. Stimuli-responsive bio-based polymeric systems and their applications. *J. Mater. Chem. B* **2019**, *7*, 709–729. [[CrossRef](#)]
28. Yang, G.; Liu, Z.; Zhang, R.; Tian, X.; Chen, J.; Han, G.; Liu, B.; Han, X.; Fu, Y.; Hu, Z.; et al. A Multi-responsive Fluorescent Probe Reveals Mitochondrial Nucleoprotein Dynamics with Reactive Oxygen Species Regulation through Super-resolution Imaging. *Angew. Chem. Int. Ed.* **2020**, *59*, 16154–16160. [[CrossRef](#)] [[PubMed](#)]
29. Guo, Z.; Song, N.R.; Moon, J.H.; Kim, M.; Jun, E.J.; Choi, J.; Lee, J.Y.; Bielawski, C.W.; Sessler, J.L.; Yoon, J. A Benzobisimidazolium-Based Fluorescent and Colorimetric Chemosensor for CO<sub>2</sub>. *J. Am. Chem. Soc.* **2012**, *134*, 17846–17849. [[CrossRef](#)] [[PubMed](#)]
30. Li, D.; Tian, X.; Liu, Z.; Liu, J.; Han, G.; Liu, B.; Zhao, J.; Zhang, R.; Tian, Y.; Zhang, Z. Revealing Sulfur Dioxide Regulation to Nucleophagy in Embryo Development by an Adaptive Coloration Probe. *Anal. Chem.* **2021**, *93*, 13667–13672. [[CrossRef](#)]
31. Yan, C.; Guo, Z.; Liu, Y.; Shi, P.; Tian, H.; Zhu, W.H. A sequence-activated AND logic dual-channel fluorescent probe for tracking programmable drug release. *Chem. Sci.* **2018**, *9*, 6176–6182. [[CrossRef](#)]
32. Yuan, L.; Lin, W.; Zheng, K.; He, L.; Huang, W. Far-red to near infrared analyte-responsive fluorescent probes based on organic fluorophore platforms for fluorescence imaging. *Chem. Soc. Rev.* **2013**, *42*, 622–661. [[CrossRef](#)] [[PubMed](#)]
33. Weissleder, R. A clearer vision for in vivo imaging. *Nat. Biotechnol.* **2001**, *19*, 316–317. [[CrossRef](#)]
34. Bu, Y.; Zhu, X.; Wang, H.; Zhang, J.; Wang, L.; Yu, Z.; Tian, Y.; Zhou, H.; Xie, Y. Self-Monitoring the Endo-Lysosomal Escape and Near-Infrared-Activated Mitophagy To Guide Synergistic Type-I Photodynamic and Photothermal Therapy. *Anal. Chem.* **2021**, *93*, 12059–12066. [[CrossRef](#)]
35. Kang, Z.; Wu, Q.; Guo, X.; Wang, L.; Ye, Y.; Yu, C.; Wang, H.; Hao, E.; Jiao, L. FeCl<sub>3</sub>-promoted regioselective synthesis of BODIPY dimers through oxidative aromatic homocoupling reactions. *Chem. Commun.* **2021**, *57*, 9886–9889. [[CrossRef](#)]
36. Wang, T.; Wang, S.; Liu, Z.; He, Z.; Yu, P.; Zhao, M.; Zhang, H.; Lu, L.; Wang, Z.; Wang, Z.; et al. A hybrid erbium(III)-bacteriochlorin near-infrared probe for multiplexed biomedical imaging. *Nat. Mater.* **2021**, *20*, 1571–1578. [[CrossRef](#)] [[PubMed](#)]
37. Yang, Q.; Jia, C.; Chen, Q.; Du, W.; Wang, Y.; Zhang, Q. A NIR fluorescent probe for the detection of fluoride ions and its application in in vivo bioimaging. *J. Mater. Chem. B* **2017**, *5*, 2002–2009. [[CrossRef](#)]
38. Zhao, X.; Yao, Q.; Long, S.; Chi, W.; Yang, Y.; Tan, D.; Liu, X.; Huang, H.; Sun, W.; Du, J.; et al. An Approach to Developing Cyanines with Simultaneous Intersystem Crossing Enhancement and Excited-State Lifetime Elongation for Photodynamic Antitumor Metastasis. *J. Am. Chem. Soc.* **2021**, *143*, 12345–12354. [[CrossRef](#)] [[PubMed](#)]
39. Li, H.D.; Yao, Q.C.; Fan, J.L.; Du, J.J.; Wang, J.Y.; Peng, X.J. An NIR fluorescent probe of uric HSA for renal diseases warning. *Dye. Pigment.* **2016**, *133*, 79–85. [[CrossRef](#)]
40. Luo, X.; Wang, R.; Lv, C.; Chen, G.; You, J.; Yu, F. Detection of Selenocysteine with a Ratiometric near-Infrared Fluorescent Probe in Cells and in Mice Thyroid Diseases Model. *Anal. Chem.* **2020**, *92*, 1589–1597. [[CrossRef](#)]
41. Yu, W.; Huang, J.; Lin, M.; Wei, G.; Yang, F.; Tang, Z.; Zeng, F.; Wu, S. Fluorophore-Dapagliflozin Dyad for Detecting Diabetic Liver/Kidney Damages via Fluorescent Imaging and Treating Diabetes via Inhibiting SGLT2. *Anal. Chem.* **2021**, *93*, 4647–4656. [[CrossRef](#)] [[PubMed](#)]
42. Zhou, K.Y.; Yang, Y.T.; Zhou, T.T.; Jin, M.; Yin, C.X. Design strategy of multifunctional and high efficient hydrogen sulfide NIR fluorescent probe and its application in vivo. *Dye. Pigment.* **2021**, *185*, 108901. [[CrossRef](#)]
43. Zhou, E.; Gong, S.; Xia, Q.; Feng, G. In Vivo Imaging and Tracking Carbon Monoxide-Releasing Molecule-3 with an NIR Fluorescent Probe. *ACS Sens.* **2021**, *6*, 1312–1320. [[CrossRef](#)] [[PubMed](#)]
44. Zeng, Z.; Ouyang, J.; Sun, L.; Zeng, C.; Zeng, F.; Wu, S. Activatable Nanocomposite Probe for Preoperative Location and Intraoperative Navigation for Orthotopic Hepatic Tumor Resection via MSOT and Aggregation-Induced Near-IR-I/II Fluorescence Imaging. *Anal. Chem.* **2020**, *92*, 9257–9264. [[CrossRef](#)]
45. Jun, Y.W.; Sarkar, S.; Kim, K.H.; Ahn, K.H. Molecular Probes for Fluorescence Imaging of ATP in Cells and Tissues. *ChemPhotoChem* **2019**, *3*, 214–219. [[CrossRef](#)]
46. Huang, B.; Liang, B.; Zhang, R.; Xing, D. Molecule fluorescent probes for adenosine triphosphate imaging in cancer cells and in vivo. *Coord. Chem. Rev.* **2022**, *452*, 214302. [[CrossRef](#)]

47. Sun, W.; Gu, X.; Dong, P.; Chu, L.; Zhang, Z.; Cheng, Z.; Yang, F. Cell-membrane-targeted near-infrared fluorescent probe for detecting extracellular ATP. *Analyst* **2022**, *147*, 4167–4173. [[CrossRef](#)]
48. Yang, B.; Qu, W.; Guo, T.; Tian, R.; Qiu, S.; Chen, X.; Geng, Z.; Wang, Z. Tetraphenylethylene fluorophore based AIE-fluorescent probe for detection of ATP in mitochondria. *Dye. Pigment.* **2023**, *215*, 111295. [[CrossRef](#)]
49. Beija, M.; Afonso, C.A.; Martinho, J.M. Synthesis and applications of Rhodamine derivatives as fluorescent probes. *Chem. Soc. Rev.* **2009**, *38*, 2410–2433. [[CrossRef](#)]
50. Chen, X.; Pradhan, T.; Wang, F.; Kim, J.S.; Yoon, J. Fluorescent chemosensors based on spiroring-opening of xanthenes and related derivatives. *Chem. Rev.* **2012**, *112*, 1910–1956. [[CrossRef](#)]
51. Li, C.Y.; Zou, C.X.; Li, Y.F.; Kong, X.F.; Zhou, Y.; Wu, Y.S.; Zhu, W.G. A colorimetric and fluorescent chemosensor for adenosine-5'-triphosphate based on rhodamine derivative. *Anal. Chim. Acta* **2013**, *795*, 69–74. [[CrossRef](#)]
52. Tang, J.L.; Li, C.Y.; Li, Y.F.; Zou, C.X. A ratiometric fluorescent probe with unexpected high selectivity for ATP and its application in cell imaging. *Chem. Commun.* **2014**, *50*, 15411–15414. [[CrossRef](#)] [[PubMed](#)]
53. Ren, T.B.; Wen, S.Y.; Wang, L.; Lu, P.; Xiong, B.; Yuan, L.; Zhang, X.B. Engineering a Reversible Fluorescent Probe for Real-Time Live-Cell Imaging and Quantification of Mitochondrial ATP. *Anal. Chem.* **2020**, *92*, 4681–4688. [[CrossRef](#)]
54. Liu, X.; Gong, X.; Yuan, J.; Fan, X.; Zhang, X.; Ren, T.; Yang, S.; Yang, R.; Yuan, L.; Zhang, X.B. Dual-Stimulus Responsive Near-Infrared Reversible Ratiometric Fluorescent and Photoacoustic Probe for In Vivo Tumor Imaging. *Anal. Chem.* **2021**, *93*, 5420–5429. [[CrossRef](#)]
55. Xu, Z.; Song, N.R.; Moon, J.H.; Lee, J.Y.; Yoon, J. Bis- and tris-naphthoimidazolium derivatives for the fluorescent recognition of ATP and GTP in 100% aqueous solution. *Org. Biomol. Chem.* **2011**, *9*, 8340–8345. [[CrossRef](#)]
56. Srivastava, P.; Razi, S.S.; Ali, R.; Srivastav, S.; Patnaik, S.; Srikrishna, S.; Misra, A. Highly sensitive cell imaging “Off-On” fluorescent probe for mitochondria and ATP. *Biosens. Bioelectron.* **2015**, *69*, 179–185. [[CrossRef](#)]
57. Ghosh, K.; Tarafdar, D.; Samadder, A.; Khuda-Bukhsh, A.R. Pyridinium-based flexible tripodal cleft: A case of fluorescence sensing of ATP and dihydrogenphosphate under different conditions and cell imaging. *RSC Adv.* **2015**, *5*, 35175–35180. [[CrossRef](#)]
58. Maity, D.; Li, M.; Ehlers, M.; Gigante, A.; Schmuck, C. A metal-free fluorescence turn-on molecular probe for detection of nucleoside triphosphates. *Chem. Commun.* **2016**, *53*, 208–211. [[CrossRef](#)] [[PubMed](#)]
59. Noguchi, T.; Shiraki, T.; Dawn, A.; Tsuchiya, Y.; Lien, L.T.N.; Yamamoto, T.; Shinkai, S. Nonlinear fluorescence response driven by ATP-induced self-assembly of guanidinium-tethered tetraphenylethene. *Chem. Commun.* **2012**, *48*, 8090–8092. [[CrossRef](#)] [[PubMed](#)]
60. Deng, T.; Chen, J.H.; Yu, H.; Yang, P.; Jian, Y.; Li, G.; Zhou, X.; Shen, H.Y.; Gui, J.Z. Adenosine triphosphate-selective fluorescent turn-on response of a novel thiazole orange derivative via their cooperative co-assembly. *Sens. Actuators B* **2015**, *209*, 735–743. [[CrossRef](#)]
61. Jiang, G.; Zhu, W.; Chen, Q.; Shi, A.; Wu, Y.; Zhang, G.; Li, X.; Li, Y.; Fan, X.; Wang, J. A new tetraphenylethylene based AIE sensor with light-up and tunable measuring range for adenosine triphosphate in aqueous solution and in living cells. *Analyst* **2017**, *142*, 4388–4392. [[CrossRef](#)] [[PubMed](#)]
62. Ma, H.; Yang, M.; Zhang, C.; Ma, Y.; Qin, Y.; Lei, Z.; Chang, L.; Lei, L.; Wang, T.; Yang, Y. Aggregation-induced emission (AIE)-active fluorescent probes with multiple binding sites toward ATP sensing and live cell imaging. *J. Mater. Chem. B* **2017**, *5*, 8525–8531. [[CrossRef](#)]
63. Ngo, H.T.; Liu, X.; Jolliffe, K.A. Anion recognition and sensing with Zn(II)-dipicolylamine complexes. *Chem. Soc. Rev.* **2012**, *41*, 4928–4965. [[CrossRef](#)] [[PubMed](#)]
64. Ojida, A.; Park, S.-k.; Mito-oka, Y.; Hamachi, I. Efficient fluorescent ATP-sensing based on coordination chemistry under aqueous neutral conditions. *Tetrahedron Lett.* **2002**, *43*, 6193–6195. [[CrossRef](#)]
65. Ojida, A.; Takashima, I.; Kohira, T.; Nonaka, H.; Hamachi, I. Turn-on fluorescence sensing of nucleoside polyphosphates using a xanthene-based Zn(II) complex chemosensor. *J. Am. Chem. Soc.* **2008**, *130*, 12095–12101. [[CrossRef](#)] [[PubMed](#)]
66. Kurishita, Y.; Kohira, T.; Ojida, A.; Hamachi, I. Rational design of FRET-based ratiometric chemosensors for in vitro and in cell fluorescence analyses of nucleoside polyphosphates. *J. Am. Chem. Soc.* **2010**, *132*, 13290–13299. [[CrossRef](#)]
67. Yan, L.W.; Ye, Z.B.; Peng, C.X.; Zhang, S.H. A new perylene diimide-based fluorescent chemosensor for selective detection of ATP in aqueous solution. *Tetrahedron* **2012**, *68*, 2725–2727. [[CrossRef](#)]
68. Singh, H.; Sreedharan, S.; Tiwari, R.; Walther, C.; Smythe, C.; Pramanik, S.K.; Thomas, J.A.; Das, A. A Fluorescent Chemodosimeter for Organelle-Specific Imaging of Nucleoside Polyphosphate Dynamics in Living Cells. *Cryst. Growth Des.* **2018**, *18*, 7199–7206. [[CrossRef](#)]
69. Jin, X.L.; Wu, X.L.; Wang, B.; Xie, P.; He, Y.L.; Zhou, H.W.; Yan, B.; Yang, J.J.; Chen, W.X.; Zhang, X.H. A reversible fluorescent probe for Zn<sup>2+</sup> and ATP in living cells and in vivo. *Sens. Actuators B* **2018**, *261*, 127–134. [[CrossRef](#)]
70. Marbumrung, S.; Wongravee, K.; Ruangpornvisuti, V.; Tumcharern, G.; Tuntulani, T.; Tomapatnaget, B. Discrimination of nucleotides by single fluorescence sensor under solvent-dependent recognition patterns. *Sens. Actuators B* **2012**, *171*, 969–975. [[CrossRef](#)]
71. Xu, Q.C.; Lv, H.J.; Lv, Z.Q.; Liu, M.; Li, Y.J.; Wang, X.F.; Zhang, Y.; Xing, G.W. A pyrene-functionalized Zinc(II)-BPEA complex: Sensing and discrimination of ATP, ADP and AMP. *RSC Adv.* **2014**, *4*, 47788–47792. [[CrossRef](#)]
72. Amendola, V.; Bergamaschi, G.; Buttafava, A.; Fabbri, L.; Monzani, E. Recognition and sensing of nucleoside monophosphates by a dicopper(II) cryptate. *J. Am. Chem. Soc.* **2010**, *132*, 147–156. [[CrossRef](#)] [[PubMed](#)]

73. Gao, Y.G.; Tang, Q.; Shi, Y.D.; Zhang, Y.; Lu, Z.L. 1,8-naphthalimide modified [12]aneN(3) compounds as selective and sensitive probes for Cu<sup>2+</sup> ions and ATP in aqueous solution and living cells. *Talanta* **2016**, *152*, 438–446. [[CrossRef](#)]
74. Andrushchenko, V.; Bour, P. Infrared absorption detection of metal ion-deoxyguanosine monophosphate binding: Experimental and theoretical study. *J. Phys. Chem. B* **2009**, *113*, 283–291. [[CrossRef](#)]
75. Nair, A.K.; Neelakandan, P.P.; Ramaiah, D. A supramolecular Cu(II) metallocyclophane probe for guanosine 5'-monophosphate. *Chem. Commun.* **2009**, *42*, 6352–6354. [[CrossRef](#)]
76. Santangelo, M.G.; Medina-Molner, A.; Schweiger, A.; Mitrikas, G.; Spingler, B. Structural analysis of Cu(II) ligation to the 5'-GMP nucleotide by pulse EPR spectroscopy. *JBIC J. Biol. Inorg. Chem.* **2007**, *12*, 767–775. [[CrossRef](#)]
77. Jin, X.; Gao, J.; Xie, P.; Yu, M.; Wang, T.; Zhou, H.; Ma, A.; Wang, Q.; Leng, X.; Zhang, X. Dual-functional probe based on rhodamine for sequential Cu(2+) and ATP detection in vivo. *Spectrochim. Acta Part A* **2018**, *204*, 657–664. [[CrossRef](#)]
78. Jin, X.L.; Wu, X.L.; Zhang, F.; Zhao, H.Q.; Zhong, W.; Cao, Y.X.; Ma, X.H.; Leng, X.; Zhou, H.W.; She, M.Y. Cu<sup>2+</sup>/ATP reversible ratiometric fluorescent probe through strip, hydrogel, and nanofiber, and its application in living cells and edaphic ecological safety assessment. *Dye. Pigment.* **2020**, *182*, 108677. [[CrossRef](#)]
79. Xiao, L.; Sun, S.; Pei, Z.; Pei, Y.; Pang, Y.; Xu, Y. A Ga(3+)-self-assembled fluorescent probe for ATP imaging in vivo. *Biosens. Bioelectron.* **2015**, *65*, 166–170. [[CrossRef](#)] [[PubMed](#)]
80. Zhang, X.; Jiang, Y.; Xiao, N. Monitoring ADP and ATP in vivo using a fluorescent Ga(III)-probe complex. *Chem. Commun.* **2018**, *54*, 12812–12815. [[CrossRef](#)] [[PubMed](#)]
81. Liu, X.; Xu, J.; Lv, Y.; Wu, W.; Liu, W.; Tang, Y. An ATP-selective, lanthanide complex luminescent probe. *Dalton Trans.* **2013**, *42*, 9840–9846. [[CrossRef](#)] [[PubMed](#)]
82. Mailhot, R.; Traviss-Pollard, T.; Pal, R.; Butler, S.J. Cationic Europium Complexes for Visualizing Fluctuations in Mitochondrial ATP Levels in Living Cells. *Chemistry* **2018**, *24*, 10745–10755. [[CrossRef](#)] [[PubMed](#)]
83. Ho, H.A.; Najari, A.; Leclerc, M. Optical detection of DNA and proteins with cationic polythiophenes. *Acc. Chem. Res.* **2008**, *41*, 168–178. [[CrossRef](#)] [[PubMed](#)]
84. Li, C.; Numata, M.; Takeuchi, M.; Shinkai, S. A sensitive colorimetric and fluorescent probe based on a polythiophene derivative for the detection of ATP. *Angew. Chem. Int. Ed.* **2005**, *44*, 6371–6374. [[CrossRef](#)]
85. Huang, B.H.; Geng, Z.R.; Ma, X.Y.; Zhang, C.; Zhang, Z.Y.; Wang, Z.L. Lysosomal ATP imaging in living cells by a water-soluble cationic polythiophene derivative. *Biosens. Bioelectron.* **2016**, *83*, 213–220. [[CrossRef](#)] [[PubMed](#)]
86. Huang, B.; Geng, Z.; Yan, S.; Li, Z.; Cai, J.; Wang, Z. Water-Soluble Conjugated Polymer as a Fluorescent Probe for Monitoring Adenosine Triphosphate Level Fluctuation in Cell Membranes during Cell Apoptosis and in Vivo. *Anal. Chem.* **2017**, *89*, 8816–8821. [[CrossRef](#)]
87. An, N.Q.; Zhang, Q.; Wang, J.; Liu, C.; Shi, L.Q.; Liu, L.H.; Deng, L.D.; Lu, Y. A new FRET-based ratiometric probe for fluorescence and colorimetric analyses of adenosine 5'-triphosphate. *Polym. Chem.* **2017**, *8*, 1138–1145. [[CrossRef](#)]
88. Tan, K.Y.; Li, C.Y.; Li, Y.F.; Fei, J.; Yang, B.; Fu, Y.J.; Li, F. Real-Time Monitoring ATP in Mitochondrion of Living Cells: A Specific Fluorescent Probe for ATP by Dual Recognition Sites. *Anal. Chem.* **2017**, *89*, 1749–1756. [[CrossRef](#)]
89. Sunnapu, O.; Kotla, N.G.; Maddiboyina, B.; Marepally, S.; Shanmugapriya, J.; Sekar, K.; Singaravadivel, S.; Sivaraman, G. Rhodamine-Based Fluorescent Turn-On Probe for Facile Sensing and Imaging of ATP in Mitochondria. *ChemistrySelect* **2017**, *2*, 7654–7658. [[CrossRef](#)]
90. Xu, Z.; Zeng, G.; Liu, Y.; Zhang, X.; Cheng, J.; Zhang, J.; Ma, Z.; Miao, M.; Zhang, D.; Wei, Y. Monitoring mitochondrial ATP in live cells: An ATP multisite-binding fluorescence turn-on probe. *Dye. Pigment.* **2019**, *163*, 559–563. [[CrossRef](#)]
91. Zhang, Z.; Chen, G.; Zhou, W.; Song, A.; Xu, T.; Luo, Q.; Wang, W.; Gu, X.S.; Duan, S. Regulated ATP release from astrocytes through lysosome exocytosis. *Nat. Cell Biol.* **2007**, *9*, 945–953. [[CrossRef](#)] [[PubMed](#)]
92. Tikum, A.F.; Kim, G.; Nasirian, A.; Ko, J.W.; Yoon, J.; Kim, J. Rhodamine-based near-infrared probe for emission detection of ATP in lysosomes in living cells. *Sens. Actuators B* **2019**, *292*, 40–47. [[CrossRef](#)]
93. Strzyz, P. Parkin and AMPK team up against necroptosis. *Nat. Rev. Mol. Cell Biol.* **2019**, *20*, 512–513. [[CrossRef](#)]
94. Tamima, U.; Sarkar, S.; Islam, M.R.; Shil, A.; Kim, K.H.; Reo, Y.J.; Jun, Y.W.; Banna, H.; Lee, S.; Ahn, K.H. A Small-Molecule Fluorescence Probe for Nuclear ATP. *Angew. Chem. Int. Ed.* **2023**, *62*, e202300580. [[CrossRef](#)]
95. Phillips, R.; Ursell, T.; Wiggins, P.; Sens, P. Emerging roles for lipids in shaping membrane-protein function. *Nature* **2009**, *459*, 379–385. [[CrossRef](#)]
96. Kurishita, Y.; Kohira, T.; Ojida, A.; Hamachi, I. Organelle-localizable fluorescent chemosensors for site-specific multicolor imaging of nucleoside polyphosphate dynamics in living cells. *J. Am. Chem. Soc.* **2012**, *134*, 18779–18789. [[CrossRef](#)] [[PubMed](#)]
97. Martens, S.; McMahon, H.T. Mechanisms of membrane fusion: Disparate players and common principles. *Nat. Rev. Mol. Cell Biol.* **2008**, *9*, 543–556. [[CrossRef](#)]
98. White, J.M. Membrane fusion. *Science* **1992**, *258*, 917–924. [[CrossRef](#)]
99. Jun, Y.W.; Wang, T.; Hwang, S.; Kim, D.; Ma, D.; Kim, K.H.; Kim, S.; Jung, J.; Ahn, K.H. A Ratiometric Two-Photon Fluorescent Probe for Tracking Lysosomal ATP: Direct In Cellulo Observation of Lysosomal Membrane Fusion Processes. *Angew. Chem. Int. Ed.* **2018**, *57*, 10142–10147. [[CrossRef](#)]
100. Wilson, W.R.; Hay, M.P. Targeting hypoxia in cancer therapy. *Nat. Rev. Cancer* **2011**, *11*, 393–410. [[CrossRef](#)]
101. Li, Y.; Sun, Y.; Li, J.; Su, Q.; Yuan, W.; Dai, Y.; Han, C.; Wang, Q.; Feng, W.; Li, F. Ultrasensitive near-infrared fluorescence-enhanced probe for in vivo nitroreductase imaging. *J. Am. Chem. Soc.* **2015**, *137*, 6407–6416. [[CrossRef](#)]

102. Fang, Y.; Shi, W.; Hu, Y.; Li, X.; Ma, H. A dual-function fluorescent probe for monitoring the degrees of hypoxia in living cells via the imaging of nitroreductase and adenosine triphosphate. *Chem. Commun.* **2018**, *54*, 5454–5457. [[CrossRef](#)] [[PubMed](#)]
103. Sies, H. Hydrogen peroxide as a central redox signaling molecule in physiological oxidative stress: Oxidative eustress. *Redox Biol.* **2017**, *11*, 613–619. [[CrossRef](#)]
104. Brand, M.D. Mitochondrial generation of superoxide and hydrogen peroxide as the source of mitochondrial redox signaling. *Free Radic. Biol. Med.* **2016**, *100*, 14–31. [[CrossRef](#)]
105. Wescott, A.P.; Kao, J.P.Y.; Lederer, W.J.; Boyman, L. Voltage-energized Calcium-sensitive ATP Production by Mitochondria. *Nat. Metab.* **2019**, *1*, 975–984. [[CrossRef](#)]
106. Majdi, S.; Larsson, A.; Najafinobar, N.; Borges, R.; Ewing, A.G. Extracellular ATP Regulates the Vesicular Pore Opening in Chromaffin Cells and Increases the Fraction Released During Individual Exocytosis Events. *ACS Chem. Neurosci.* **2019**, *10*, 2459–2466. [[CrossRef](#)]
107. Wu, Z.; Liu, M.; Liu, Z.; Tian, Y. Real-Time Imaging and Simultaneous Quantification of Mitochondrial H<sub>2</sub>O<sub>2</sub> and ATP in Neurons with a Single Two-Photon Fluorescence-Lifetime-Based Probe. *J. Am. Chem. Soc.* **2020**, *142*, 7532–7541. [[CrossRef](#)]
108. Valez, V.; Cassina, A.; Batinic-Haberle, I.; Kalyanaraman, B.; Ferrer-Sueta, G.; Radi, R. Peroxynitrite formation in nitric oxide-exposed submitochondrial particles: Detection, oxidative damage and catalytic removal by Mn-porphyrins. *Arch. Biochem. Biophys.* **2013**, *529*, 45–54. [[CrossRef](#)] [[PubMed](#)]
109. Uribe, P.; Treulen, F.; Boguen, R.; Sanchez, R.; Villegas, J.V. Nitrosative stress by peroxynitrite impairs ATP production in human spermatozoa. *Andrologia* **2017**, *49*, e12615. [[CrossRef](#)] [[PubMed](#)]
110. Graves, J.E.; Lewis, S.J.; Kooy, N.W. Role of ATP-sensitive K<sup>+</sup> -channels in hemodynamic effects of peroxynitrite in anesthetized rats. *J. Cardiovasc. Pharmacol.* **2005**, *46*, 653–659. [[CrossRef](#)] [[PubMed](#)]
111. Wu, L.; Liu, J.; Tian, X.; Groleau, R.R.; Feng, B.; Yang, Y.; Sedgwick, A.C.; Han, H.H.; Wang, Y.; Wang, H.M.; et al. Dual-Channel Fluorescent Probe for the Simultaneous Monitoring of Peroxynitrite and Adenosine-5'-triphosphate in Cellular Applications. *J. Am. Chem. Soc.* **2022**, *144*, 174–183. [[CrossRef](#)] [[PubMed](#)]
112. Hinson, J.A.; Roberts, D.W.; James, L.P. Mechanisms of acetaminophen-induced liver necrosis. *Handb. Exp. Pharmacol.* **2010**, *196*, 369–405. [[CrossRef](#)]
113. Jiang, W.L.; Wang, W.X.; Wang, Z.Q.; Tan, M.; Mao, G.J.; Li, Y.; Li, C.Y. A tumor-targeting near-infrared fluorescent probe for real-time imaging ATP in cancer cells and mice. *Anal. Chim. Acta* **2022**, *1206*, 339798. [[CrossRef](#)] [[PubMed](#)]

**Disclaimer/Publisher's Note:** The statements, opinions and data contained in all publications are solely those of the individual author(s) and contributor(s) and not of MDPI and/or the editor(s). MDPI and/or the editor(s) disclaim responsibility for any injury to people or property resulting from any ideas, methods, instructions or products referred to in the content.